Highlights:

1) Simple coupled sea ice – ocean model has been developed to simulate the seasonal cycle of sea ice formation.
2) Salt flux associated with the wind-forced ice production causes haline convection affecting the characteristics of the entire water column.
3) The comparison between model-derived polynya extents and MODIS IST images was performed.
4) High resolution wind forcing is necessary to capture in more detail coastal sea ice processes, such as coastal polynyas, ice drift and ice compression against coastline features.

Modelling sea ice formation in the Terra Nova Bay polynya

Sansiviero M.[1], Morales Maqueda M. Á.[2,3], Fusco G.[1], Aulicino G.[1], Flocco D.[4] and Budillon G.[1]

[1] Università degli Studi di Napoli "Parthenope" (Italy)

[2] School of Marine Science and Technology, Newcastle University (United Kingdom)

[3] National Oceanography Centre (United Kingdom)

[4] Centre for Polar Observation and Modelling, University of Reading (United Kingdom)

Corresponding author: manuela.sansiviero@uniparthenope.it

Abstract

Antarctic sea ice is constantly exported from the shore by strong near surface winds that open leads and large polynyas in the pack ice. The latter, known as wind-driven polynyas, are responsible for significant water mass modification due to the high salt flux into the ocean associated with enhanced ice growth. In this article, we focus on the wind-driven Terra Nova Bay (TNB) polynya, in the western Ross Sea. Brine rejected during sea ice formation processes that occur in the TNB polynya densifies the water column leading to the formation of the most characteristic water mass of the Ross Sea, the High Salinity Shelf Water (HSSW). This water mass, in turn, takes part in the formation of Antarctic Bottom Water (AABW), the densest water mass of the world ocean, which plays a major role in the global meridional overturning circulation, thus affecting the global climate system. A simple coupled sea ice – ocean model has been developed to simulate the seasonal cycle of sea ice formation and export within a polynya. The sea ice model accounts for both thermal and mechanical ice processes. The oceanic circulation is described by a one-and-a-half layer, reduced gravity model. The domain resolution is $1\ \text{km} \times 1\ \text{km}$, which is sufficient to represent the salient features of the coastline geometry, notably the Drygalski Ice Tongue. The model is forced by a combination of Era Interim reanalysis and in-situ data from automatic weather stations, and also by a climatological oceanic dataset developed from in situ hydrographic observations. The sensitivity of the polynya to the atmospheric forcing is well reproduced by the model when atmospheric in situ measurements are combined with reanalysis data. Merging the two datasets allows us to capture in detail the strength and the spatial distribution of the katabatic winds that often drive the opening of the polynya. The model resolves fairly accurately the sea ice drift and sea ice production rates in the TNB polynya, leading to realistic polynya extent estimates. The model-derived polynya extent has been validated by comparing the modelled sea ice concentration against MODIS high resolution satellite images, confirming that the model is able to reproduce reasonably well the TNB polynya evolution in terms of both shape and extent.

1. Introduction

Observations and models have clearly shown that changes in atmospheric forcing and ocean circulation affect the Antarctic sea ice extent (Jacobs and Comiso, 1997; Liu et al., 2004; Lefebvre et al., 2005; Zhang 2007; Turner et al., 2009; Liu and Curry, 2010). The pronounced pattern of increasing ice cover in the Ross Sea region, found to be the highest contributor to sea ice expansion amongst the five Southern Ocean sectors in the 1979 - 2010 period with a positive trend of 13700 ± 1500 km^2 yr^{-1}, has been ascribed to changes in atmospheric circulation (Parkinson and Cavalieri, 2012). Enhanced northward winds have changed sea ice drift and export offshore affecting the dynamics of the local oceanography. These changes impact on the occurrence of wind driven polynyas along the Antarctic coastal margin, modifying the production of dense water masses through sea ice growth (Holland and Kwok, 2012). Variation in size or extent of polynyas are believed to be suitable indicators of climatic change (Morales Maqueda et al., 2004).

The wind-driven Terra Nova Bay (TNB) polynya, located in the western sector of the Ross Sea, plays a major role in shaping the sea ice and ocean dynamics of this region (Kurtz and Bromwich, 1985; Bromwich, 1989). The polynya opening results principally from the synergy of meteorological, oceanographic, and physical geography features of this region (Fig.1). Especially during winter, the TNB polynya is frequently forced by cold and strong katabatic downslope flows that push sea ice away from the coast. Their action prevents sea ice from consolidating as a thick pack and, at the same time, facilitates its continuous formation by leaving the relatively warm open water exposed to the cold atmosphere. Also, the presence and the orientation of the Drygalski Ice Tongue is essential for the polynya maintenance, since this barrier blocks the incoming sea ice from the south and controls, through its length, the polynya extent (Frezzotti and Mabin, 1994). Due to the constant formation and offshore drift of new ice, the TNB polynya contributes significantly to the sea ice mass budget of the whole area, producing approximately 10% of the sea ice formed annually in the Ross Sea (Kurtz and Bromwich, 1985; Van Woert, 1999b). Associated with the wind-forced ice production is a salt flux that causes haline convection that affects the characteristics of the entire water column in the TNB polynya and the thermohaline structure of the whole Ross Sea (Kurtz and Bromwich, 1985; Trumbore et al., 1991). The TNB polynya is considered to be by far the largest producer of High Salinity Shelf Water (HSSW) (Kurtz and Bromwich, 1983, 1985; Jacobs et al., 1985; Van Woert, 1999a, b; Budillon and Spezie, 2000; Budillon et al., 2003; Fusco et al., 2009), a water mass that plays a crucial role in the formation of Antarctic Bottom Water (AABW) (Kurtz and Bromwich, 1985; Jacobs and Comiso, 1989; Van Woert, 1999a), thus contributing to deep ocean ventilation and the global thermohaline circulation (Jacobs et al., 1985; Orsi et al., 1999; Jacobs 2004).

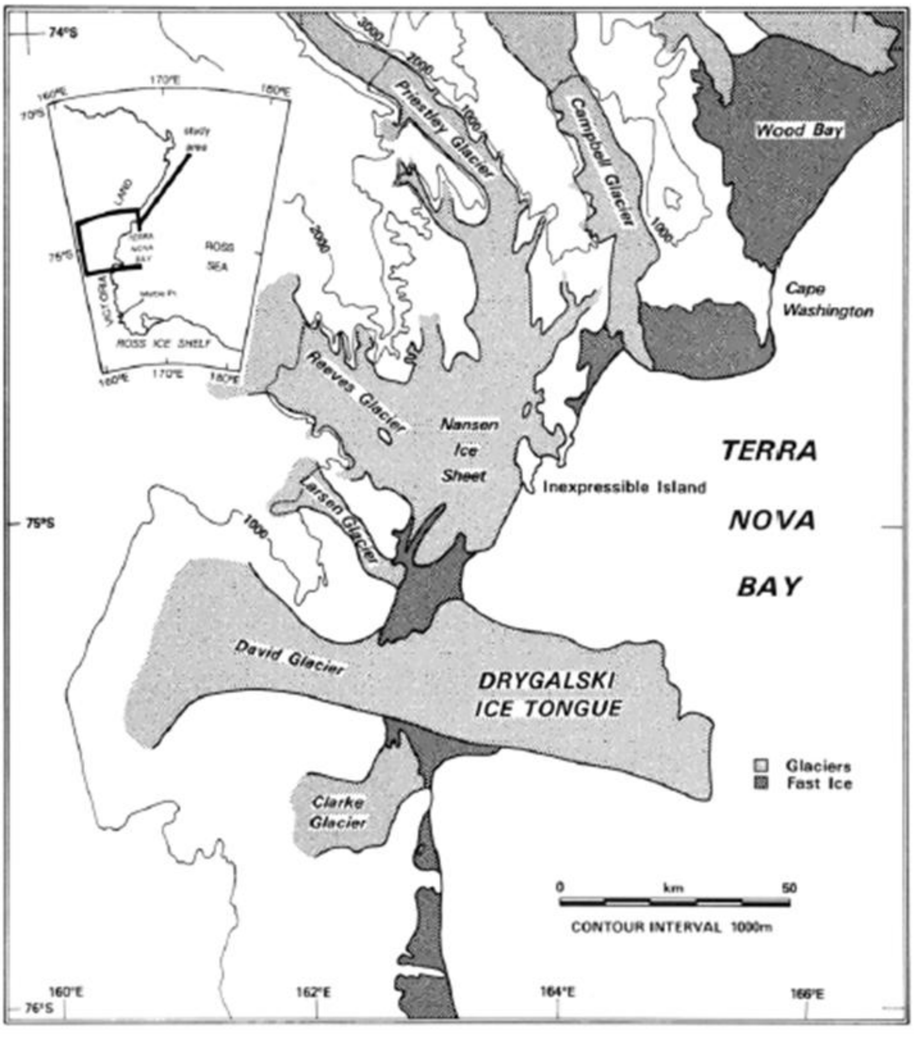

Fig. 1: Overview map of TNB (Western Ross Sea) showing the major geographical features of this region and its surroundings (Kurtz and Bromwich, 1983).

The main goal of this study is to investigate the sea ice behaviour in the Terra Nova Bay polynya in response to external forcing and to estimate the associated sea ice and HSSW production. To this purpose, a coupled sea ice – ocean model was developed and applied to the TNP polynya area. The model simulates the seasonal cycle of sea ice formation in the TNB polynya, accounting for both sea ice dynamic and thermodynamic processes. Dynamics does not produce ice directly, but causes the ice to drift in and out of the area and leads to ice deformation in form of rafting or ridging due to convergence. Thermodynamics processes are responsible for local ice growth or melt and heat transfer at the ice-air and ice-ocean interfaces (Rothrock, 1979). Both ice dynamics and thermodynamics alter the local mean thickness (ice volume per unit area) and result in the exchange of mass, momentum and energy with the atmosphere and the ocean (Flato, 2003).

A further goal of this work is to estimate the variation of the TNB polynya extent, i.e. the size of the area of low ice concentration, in response to the forcing. Computing the polynya extent is difficult given the limitations of models and remote sensing tools as regards both their accuracy and their ability to resolve polynya variability in space and time. Polynya extent estimates are not trivial to derive since local ice thickness and ice production rates are often unknown. Papers focusing on the variability of sea ice and open water in the TNB polynya exist in literature, mainly concerning the wintertime season. Authors have investigated the TNB polynya extent either through one dimensional models forced by in situ and reanalysis data (Van Woert, 1999a, 1999b; Fusco et al., 2002; Petrelli et al., 2008) or through satellite observations (Kern, 2007; Ciappa et al., 2012).

The polynya extent in this paper is derived from modelled sea ice concentration (Markus et al., 1998; Kwok et al., 2007; Tamura et al., 2008) and validated by comparison with polynya extents estimates from MODIS satellite images (Key et al., 1994; Key et al., 1997).

The paper is organized as follows. Section 2 provides a description of the coupled sea ice – ocean model and the main formulations adopted to resolve sea ice dynamics and thermodynamics. Section 3 presents experiments on model sensitivity to variations in specific physical processes and parameterizations in order to better tune the model to the peculiarities of the TNB polynya region.

In particular, the sea ice and polynya response to wind forcing variations is studied. Section 4 shows the results of a one year simulation of sea ice formation and polynya extent in the TNB polynya region. Section 5 focuses on the comparison between the numerical TNB polynya extent estimates and those derived from high resolution MODIS images. Finally, a discussion of results and a few concluding remarks are presented in Section 6.

2. Description of the model

2.1 Model equations

The coupled sea ice – ocean model presented here provides an intermediate complexity formulation of the TNB polynya dynamics. In contrast by polynya flux models describing the evolution of a polynya in terms of the polynya edge contour, our model predicts sea ice concentrations over a regular spatial grid (Willmott et al., 2007). The model has a relatively high resolution (1 km × 1 km) in order to capture the complexity of the coastline geometry and the meteorological patterns of the region. Both dynamic and thermodynamic sea ice and ocean processes are incorporated in the model. An accurate representation of the main sea ice processes, often overlooked in numerical simulations of the polar regions (Russell et al., 2006; Maksym et al., 2012), and a realistic representation of sea ice dynamics, are crucial for the accurate description of the interactions of thin ice and polynyas with the atmospheric and oceanic circulation (Stössel et al, 1990). The ocean is represented by a one-and-a-half layer, reduced gravity, Boussinesq ocean model. The stratification is simplified using a description in which the active layer (effectively, the upper ocean mixed layer) moves above a lower stagnant (motionless) layer of infinite depth. The formulation of the ocean model is inspired in Morales Maqueda et al. (1999) and Biggs and Willmott (2001), with the only major departure that an eddy bolus transport term is added to the advection of scalars. The equations are as follows.

$$h_1\left(\frac{\partial U_1}{\partial t}+\frac{\partial (U_1U_1)}{\partial x}+\frac{\partial (V_1U_1)}{\partial y}\right)-fh_1V_1=-\frac{\partial}{\partial x}\left(\frac{1}{2}g\,\frac{\rho_r-\rho_1}{\rho_r}h_1^2\right)+\frac{1}{\rho_r}\,(\tau_s^x-\,\tau_b^x)+\frac{1}{\rho_r}\left(\frac{\partial}{\partial x}\left(A_H h_1\frac{\partial U_1}{\partial x}\right)+\frac{\partial}{\partial y}\left(A_H h_1\frac{\partial U_1}{\partial y}\right)\right), \tag{1}$$

$$h_1\left(\frac{\partial V_1}{\partial t}+\frac{\partial (U_1V_1)}{\partial x}+\frac{\partial (V_1V_1)}{\partial y}\right)+fh_1U_1=-\frac{\partial}{\partial y}\left(\frac{1}{2}g\,\frac{\rho_r-\rho_1}{\rho_r}h_1^2\right)+\frac{1}{\rho_r}\,(\tau_s^y-\,\tau_b^y)+\frac{1}{\rho_r}\left(\frac{\partial}{\partial x}\left(A_H h_1\frac{\partial V_1}{\partial x}\right)+\frac{\partial}{\partial y}\left(A_H h_1\frac{\partial V_1}{\partial y}\right)\right), \tag{2}$$

$$\frac{\partial h_1}{\partial t}=-\left\{\frac{\partial[h_1(U_1+U_e)]}{\partial x}+\frac{\partial[h_1(V_1+V_e)]}{\partial y}\right\}-E+P+M_s+M_i-G_i+w_b, \tag{3}$$

$$\frac{\partial (h_1T_1)}{\partial t}=-\left\{\frac{\partial[h_1T_1(U_1+V_e)]}{\partial x}+\frac{\partial[h_1T_1(V_1+V_e)]}{\partial y}\right\}+\frac{Q_1+Q_i}{\rho_r c_p}+w_bT_b+h_1\frac{T_c-T_1}{\mathrm{T}_r}, \tag{4}$$

$$\frac{\partial (h_1S_1)}{\partial t}=-\left\{\frac{\partial[h_1S_1(U_1+U_e)]}{\partial x}+\frac{\partial[h_1S_1(V_1+V_e)]}{\partial y}\right\}+(M_i-G_i)S_i+w_bS_b+h_1\frac{S_c-S_1}{\mathrm{T}_r}. \tag{5}$$

In the equations above, h_1 is the depth of the ocean active layer, U_1 and V_1 are the x and y components of the ocean current in the active layer, $\mathbf{U}_1$, f is the Coriolis parameter, g is the acceleration of gravity, ρ_r is a constant and uniform reference density representative on average of the densities encountered in the region below the active layer, ρ_1 is the density of the active layer, τ_s^x and τ_s^y are the components of the horizontal wind stress at the top of the active layer and, similarly, τ_b^x and τ_b^y are the components of the vertical shear stress at the bottom of the active layer, $U_e=-\kappa_e h_1^{-1}\,\partial h_1/\partial x$ and $V_e=-\kappa_e h_1^{-1}\,\partial h_1/\partial y$ are the components of the eddy bolus velocity (Gent and McWilliams, 1990), with κ_e a constant and uniform thickness diffusivity, E is evaporation, P is precipitation, M_s and M_i are the volume fluxes associated with snow and ice melt, respectively, G_i is ice growth (exception made of snow ice formation, which is described below), w_b represents the vertical volume flux at the base of the active layer caused by entrainment, T_1 is the temperature of the active layer, and Q_1 is the net surface heat flux into the layer, incorporating contributions from the ice free and ice covered areas and also including the latent heat loss required to melt the snow that falls over leads. Specifically,

$$Q_1 = (1 - A)\left(Q_{sw} + Q_{lw} + Q_s + Q_e - P\, L_f \rho_s\right) - AQ_c \tag{6}$$

where A is the fractional oceanic area covered by ice, or ice concentration, Q_{sw}, Q_{lw}, Q_s and Q_e are the shortwave, longwave, sensible and latent heat fluxes in the open ocean, the four quantities positive if they flow into the ocean and calculated according to Budillon et al. (2000), L_f is the latent heat of fusion of ice, ρ_s is snow density, and Q_c is the conductive heat flux through ice, which we take as positive if directed upwards and assume to be identical to the heat flux from the ocean into the ice at the base of the ice cover. Small enthalpy changes associated with the mass fluxes E, P, M_s, M_i and G_i are all ignored here since we neglect the thermal inertia of both snow and ice. Further in (4), Q_i is a latent heat flux associated with the formation or melting of ice in the active oceanic layer (see below) and T_b is the temperature associated with the volume flux w_b across the base of the active layer. The last term on the right hand side of (4) represents a relaxation to observations, T_c, with a time scale T_r. In (5), S_1 is the salinity of the active layer and S_i and S_b are the salinity of sea ice, which we take as constant and equal to 4, and the salinity of water entrained at the base of the active layer, respectively. Relaxation to salinity observations, S_c, is also included. The temperature T_1 is approximately maintained at the freezing point, T_f, which is calculated according to Fofonoff and Millard (1983), for as long as ice is present or if ice forms for the first time in the season in the open ocean. The term Q_i in (4) ensures this, and it has the form

$$Q_i = \rho_r c_p \left\{H(A) + [1 - H(A)]H\left(T_f - T_1\right)\right\} h_1 \frac{T_f - T_1}{\mathrm{T}_i}. \tag{7}$$

In (7), H is the Heaviside function, A is the ice concentration, and T_i is a restoring time scale which we have chosen to be equal to the model time step. The entrainment velocity, w_b, depends on the air-sea stress and buoyancy fluxes that control the strength of turbulence in the mixed layer and is parameterized according to Lemke (1987) as

$$w_b = \frac{2\, u^{*3} e^{-h_1/h_w} + h_1 B\left[1 + H(B)\left(e^{-h_1/h_c} - 1\right)\right]}{g \frac{\rho_r - \rho_1}{\rho_r} h_1} \tag{8}$$

where $\rho_r u^{*2} = \sqrt{\tau_s^{x2} + \tau_s^{y2}}$, $h_w = 7\,m$, B is the surface buoyancy flux, and $h_c = 50\,m$. The temperature and salinity of entrained water, T_b and S_b, are determined using mooring based observations (see Section 2.3) linearly interpolated onto the bottom of the active layer.

The surface stress term is formulated as in Mellor and Kantha (1989) and is a linear combination of the shear stress at the surface of the ice covered ocean and the wind stress acting on the open ocean, weighted by the fractional area of sea ice and leads, respectively, namely, $\tau_s^x = (1-A)\tau_{sw}^x + A\tau_{si}^x$, where τ_{sw}^x is the *x* component of the surface stress over the ocean and τ_{si}^x is the sea ice counterpart. An analogous equation holds for τ_s^y. In full, the ice-ocean stress components are

$$\left(\tau_{si}^x, \tau_{si}^y\right) = \rho_i C_i \sqrt{(U_1 - U_i)^2 + (V_1 - V_i)^2}(U_i - U_1, V_i - V_1), \tag{9}$$

where $C_i = 5 \times 10^{-3}$ is the ice-ocean drag coefficient, and U_i and V_i are the components of the ice velocity. The stress at the base of the active layer is calculated according to the parameterization of Pacanowski and Philander (1981):

$$\left(\tau_b^x, \tau_b^y\right) = \left(\nu_b + \frac{\nu_0}{(1+\alpha\, Ri)^n}\right)\frac{1}{h_1}(U_1, V_1), \tag{10}$$

where $\nu_b = 1 \times 10^{-3} m^2 s^{-1}$, $\nu_0 = 1 \times 10^{-1} m^2 s^{-1}$, $\alpha = 0.5$, $n = 2$ and Ri is a Richardson number:

$$Ri = \frac{g\frac{\rho_r - \rho_1}{\rho_r}h_1}{u_1^2 + v_1^2}. \tag{11}$$

The horizontal friction terms in (1) and (2) are included to make it possible to impose no-slip boundary conditions at coastlines. The viscosity, A_H, has a value of 2×10^2 m^2 s^{-1}.

Sea ice behaves as a floating, zero layer system (i.e., without thermal inertia), as proposed by Semtner (1976). Sea ice interacts thermodynamically and dynamically with the atmosphere and the underlying mixed layer of the ocean. The coupling of sea ice with the surface ocean layer allows us to simulate the seasonal cycle of sea ice formation and export within the polynya. The model requires atmospheric and ocean forcing as inputs that are applied as surface and bottom boundary conditions. The atmospheric forcing is given by air temperature, surface pressure, humidity, cloud cover, precipitation and wind fields, from which surface heat, moisture and momentum fluxes can be derived. The model needs also the solar radiation in order to compute the balance of radiative and the turbulent heat fluxes. The ocean forcing consists of the ocean surface temperatures and salinities. The main variables involved in the coupled sea ice-ocean model are shown in Fig. 2 as well as a schematic decomposition of the heat balance at the air-ocean, air-ice and ice-ocean interfaces.

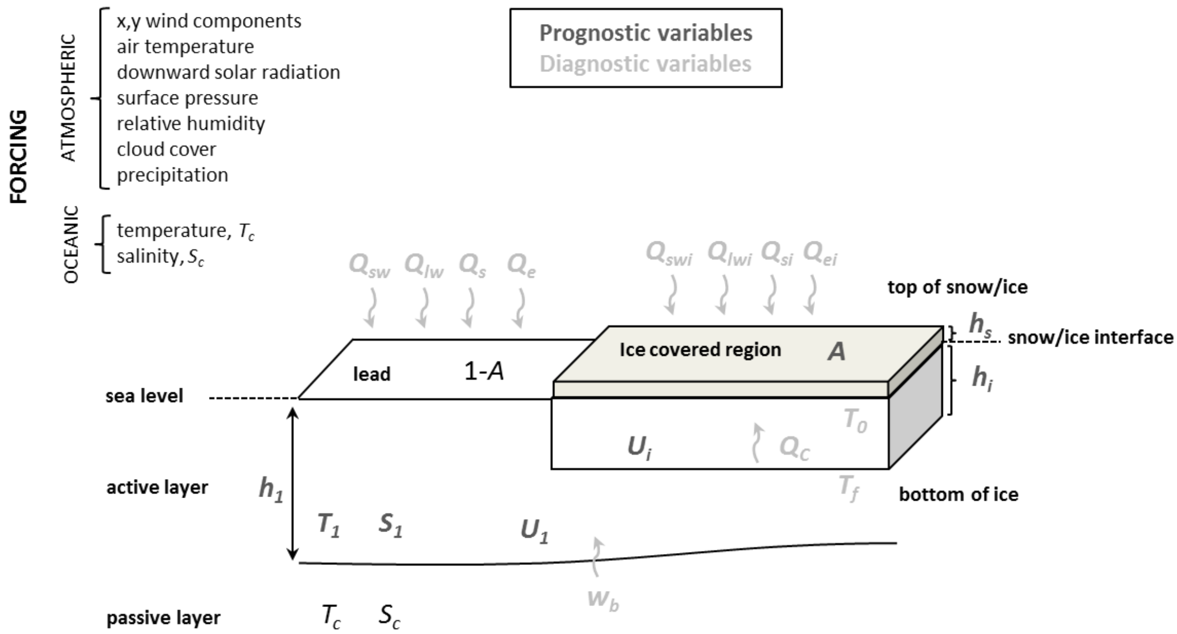

Fig. 2: Schematic view of the main variables of the coupled sea ice – ocean model. The radiative and turbulent heat fluxes are separately calculated over the ice free (leads) and ice covered areas.

The sea ice state is characterized by the ice concentration, A, defined as the fraction of a grid cell covered by ice varying between zero and one, and by the ice thickness, h_i. The non-covered fraction of each grid cell, $1 - A$, is referred to as the lead fraction. Sea ice is allowed to be covered by a snow layer, h_s, that is important for the determination of the growth rates of sea ice (Stössel et al., 1990). Also, snow-ice formation from Fichefet and Morales Maqueda (1999), which takes part in the thickening of sea ice when the snow layer is depressed below the sea surface by its own weight, is parameterized. The conservation equations for the sea ice and snow state variables are as follows.

$$\frac{\partial A}{\partial t} == -\left\{\frac{\partial (Au_i)}{\partial x} + \frac{\partial (Av_i)}{\partial y}\right\} + S_A, \tag{12}$$

$$\frac{\partial (Ah_i)}{\partial t} = -\left\{\frac{\partial (Ah_i u_i)}{\partial x} + \frac{\partial (Ah_i v_i)}{\partial y}\right\} + \dot{V}_i + \dot{V}_{i0} + \dot{V}_{si}, \tag{13}$$

$$\frac{\partial (Ah_s)}{\partial t} = -\left\{\frac{\partial (Ah_s u_i)}{\partial x} + \frac{\partial (Ah_s v_i)}{\partial y}\right\} + \dot{V}_{s0} - \frac{\rho_i}{\rho_s}\dot{V}_{si}, \tag{14}$$

where u_i and $v_i$are the components of the sea ice velocity. The term S_A is a placeholder for all non-advective processes that lead to changes in ice concentration. It is formulated in the following way.

$$S_A = (1 - A)\frac{Q_i/\left(L_f \rho_i\right)}{d}, \tag{15}$$

where, L_f is the latent heat of formation of ice, and, if $Q_i > 0$ (i.e., there is frazil ice formation in the water column), d is a collection thickness of frazil ice which is either a constant or a function of wind speed as in Winsor and Bjork (2000), and we denote it by H, while, if $Q_i < 0$, $d = h_i$. The terms $\dot{V}_i = Q_i/\left(L_f \rho_i\right)$, $\dot{V}_{i0}$ and $\dot{V}_{si}$in (13) account for ice growth/decay as a result of the heat budget in the active oceanic layer, for sea ice melting at the ice-atmosphere interface when the ice heat balance is such that the surface is at the melting point, and for snow ice formation, respectively. We note that the term G_i in (3) is simply equal to ${}^{\rho_i}/_{\rho_r}\,\dot{V}_i$. Snow ice formation occurs when the weight of snow depresses the snow-ice interface below sea level. In such cases, we transform the submerged snow into ice, leading to a contribution to the ice growth rate that obeys the formula

$$\dot{V}_{si} = \frac{A}{\mathrm{T}_{si}}\, H\left(\frac{\rho_s h_s - (\rho_r - \rho_i) h_i}{\rho_r}\right)\frac{\rho_s}{\rho_i}\frac{\rho_s h_s - (\rho_r - \rho_i) h_i}{\rho_r}, \tag{16}$$

where T_{si} is a time scale that we take to be equal to the time step in the model. The term $\dot{V}_{s0}$ in (14) accounts for both the accumulation of precipitating snow on top of sea ice and the subsequent surface snow melt during the thaw. As stated above, we make use of an approach for the sea ice and snow thermodynamics that is commonly termed zero layer approximation. This means that the vertical temperature profiles in the snow and the ice are linear and fully determined by the temperatures at their respective top and bottom interfaces. At the ice-ocean interface, the temperature is always taken to be T_f, and we further assume that the oceanic heat flux into the ice matches the conductive heat flux through the ice, Q_c, so that there is never a flux divergence at the bottom of the ice cover. At the ice-snow interface, the conductive heat flux is also assumed to be continuous. The conductive heat flux is given by the following expression (e.g., Fichefet and Morales Maqueda, 1997):

$$Q_c = \frac{\kappa_i}{h_i + \frac{\kappa_i}{\kappa_s} h_s}\left(T_f - T_0\right), \quad (17)$$

where κ_i and κ_s are the heat conductivities of ice and snow, respectively, and T_0 is the surface temperature. Finally, at the surface of the ice or snow cover a balance is postulated between surface and conductive heat fluxes, namely,

$$Q_0 = Q_{swi} + Q_{lwi} + Q_{si} + Q_{ei} + Q_c = 0, \quad (18)$$

where Q_{swi}, Q_{lwi}, Q_{si} and Q_{ei} are the shortwave, longwave, sensible and latent heat fluxes at the surface of the snow or ice layer. The balance $Q_0 = 0$ in (18) can be guaranteed as long as T_0 remains below the freezing point. However, if (18) requires that the surface temperature be above freezing then melting will ensure. During melting, T_0 will remain at the freezing point for freshwater (if snow is present) or for ice (if there is no snow) and the excess heat $Q_0 > 0$ will be used to melt snow, $M_s = Q_0/\left(L_f \rho_s\right)$, or ice $M_i = Q_0/\left(L_f \rho_i\right)$.

Sea ice drift, $\mathbf{U}_i$, with components U_i and V_i, is computed by postulating a balance of momentum between the Coriolis force, wind and ocean stresses and the ice internal force resulting from the interaction between floes during ice deformation. The momentum equations are:

$$m\frac{\partial U_i}{\partial t} - fmV_i = A(\tau_w^x - \tau_o^x) + F^x, \quad (19)$$

$$m\frac{\partial V_i}{\partial t} + fmU_i = A\left(\tau_w^y - \tau_o^y\right) + F^y, \quad (20)$$

where m is the mass of snow plus ice per unit area, τ_w^x and τ_w^y are the components of the wind stress acting on the ice, τ_o^x and τ_o^y are the components of the ice-ocean stress at the base of the ice, and F^x and F^y are the components of the ice internal stress force. Note that advection of sea ice momentum is ignored and that the atmosphere and ocean stresses term includes the ice concentration as a multiplicative factor to be consistent with the theory of free drift in regions of low ice concentration according to Connolley et al. (2004). The internal ice forces are resolved using the elastic-viscous-plastic rheology by Hunke and Dukowicz (1997). The internal ice pressure is formulated as a function of sea ice thickness, h_i, and concentration, A, as in Hibler (1979) (see further discussion in section 3.1).

2.2 Model domain and set up

The model domain consists of a wide region of the western Ross Sea including an extended area along the coast of Victoria Land south of the Drygalski Ice Tongue and the northern region of the Wood Bay (Fig. 3). It is 154 km × 488 km, extending approximately from 74°S to 78°S in latitude and from 162°E to 168°E in longitude. A spatially uniform horizontal resolution of 1 km is used to study the small scale behaviour of sea ice in TNB. This resolution is considered to be sufficient in representing the salient features of the coastline geometry, such as the Drygalski Ice Tongue. Hence, the horizontal grid is a rectangle of width X and length Y subdivided in square grid cells resulting in a grid of 154 × 488 = 75152 grid points. An Arakawa B-grid is used for the spatial discretization. A land mask is specified in the center of the cells with 0 representing land and 1 oceanic cells. A corresponding mask is defined for all corner quantities such as the wind speed, sea ice velocity and stress components.

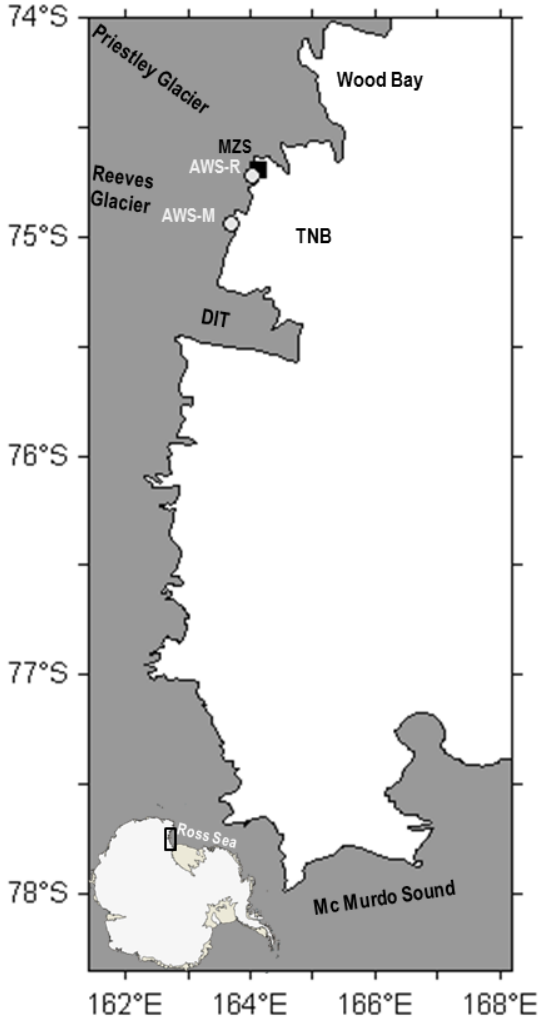

Fig. 3: The model domain showing the Drygalski Ice Tongue (DIT) and the two preferential paths of the katabatic flows, the Priestley and the Reeves Glaciers. The italian base, Mario Zucchelli Station (MZS), and the location of the automatic weather stations, Rita (AWS-R: 74.72°S, 164.03°E) and Manuela (AWS-M: 74.95°S, 163.69°E) are also indicated.

The advection of scalars is discretized with a first order upstream scheme. The solutions of the momentum equations (1), (2), (19) and (20) and the advective and thermodynamic processes in eqs. (3), (4), (5), (12), (13) and (14) are computed using two different time steps: a small one for the momentum (Δt) and a larger one for the advection(ΔT_a). All the input parameters such as constants and coefficients are shown in Table 1. Some values of the input parameters, referred to as "x" in Table 1, are let to vary in the sensitivity experiments. A one month spin-up length (repeated twice) is used for each experiment. Sea ice concentration and thickness and ocean fields are initialized at the beginning of each integration with a prescribed value or with a restart from a previous integration. The initial values are zero for both ice concentration and thickness. The initial temperature and salinity of the ocean are from monthly climatological observations (described in section 2.3) and the initial active layer depth is determined from the former using the density threshold criterion of 0.125 kg m^{-3} relative to near surface densities (Monterey and Levitus, 1997). Open lateral boundary conditions ensuring a minimum of signal reflections at the boundary have been used so that advective flows leaving the domain are allowed to freely exit the domain using an upstream formulation, while flows into the domain use a simple sponge boundary condition that relaxes the variables to their climatological external values (Martinsen and Engedahl, 1987). The main physical parameters of atmosphere, sea ice and ocean used in the model are showed in Table 2. Figure 4 is the flow diagram of the coupled sea ice-ocean model, showing the basic steps in computing the diagnostic variables of the model.

Parameter	**Symbol**	**Value**
X domain	X	154000 m
Y domain	Y	488000 m
T domain	T	x days
Time step for momentum	Δt	1.2 s
Time step for advection	Δt_a	600 s
Elastic timescale (EVP ice rheology)	Δte	180 s
Air drag coefficient	C_{da}	x
Ocean drag coefficient	C_{do}	x
Ice strength parameter	P^*	x N/m^2
Ice concentration parameter	C	20
Creep limit	c	5×10^{-11} 1/s
Eccentricity of the elliptical yield curve	e	2
Demarcation ice collection thickness in leads	H	x m

Table 1: Input parameters of the model. The “x” stands for a varying value assigned to that parameter in the sensitivity experiments.

Parameter	Symbol	Value
Ocean horizontal viscosity	A_H	$2 \times 10^2 \mathrm{m}^2 \mathrm{s}^{-1}$
Ocean eddy thickness diffusivity	κ_e	$2 \times 10^2 \mathrm{m}^2 \mathrm{s}^{-1}$
Thermal conductivity of sea ice	κ_i	2.2 W/m/K
Thermal conductivity of snow	κ_s	0.3 W/m/K
Emissivity of atmosphere	ε_a	0.95
Emissivity of ocean	ε_o	0.985
Albedo of ocean	α_o	0.07
Albedo of ice	α_i	0.07-0.7
Albedo of snow	α_{sn}	0.85
Latent heat of fusion of ice	L_{fi}	3.34×10^5 J/kg
Latent heat of vaporization of water	L_e	2.5×10^6 J/kg
Latent heat of fusion of snow	L_{fsn}	3.34×10^5 J/kg
Latent heat of sublimation of snow	L_{ssn}	2.834×10^6 J/kg
Specific heat capacity of ocean	c_{pa}	3985 J/kg/K
Specific heat capacity of air	c_{pa}	1004 J/kg/K
Density of air	ρ_a	1.3 $\mathrm{Kg/m^3}$
Density of ice	ρ_i	900 $\mathrm{Kg/m^3}$
Density of snow	ρ_s	330 $\mathrm{Kg/m^3}$
Density of ocean	ρ_o	1024 $\mathrm{Kg/m^3}$
Melting point of freshwater ice	t_{fus}	0°C
Salinity of sea ice	s_i	4
Exchange coeff. for sensible heat (leads/ice)	c_H	1.75×10^{-3}
Exchange coeff. for latent heat over leads	c_E	1.75×10^{-3}
Exchange coeff. for latent heat over ice	c_E	1×10^{-3}
Stefan-Boltzmann constant	K	5.67×10^{-8} W m^{-2} K^{-4}
Minimum vertical viscosity	υ_{min}	1×10^{-3} $\mathrm{m}^2 \mathrm{s}^{-1}$
Scale depth of mechanical dissipation	h_w	7 m
Scale depth of convective dissipation	h_c	50 m

Table 2: Physical parameters of atmosphere, sea ice and ocean.

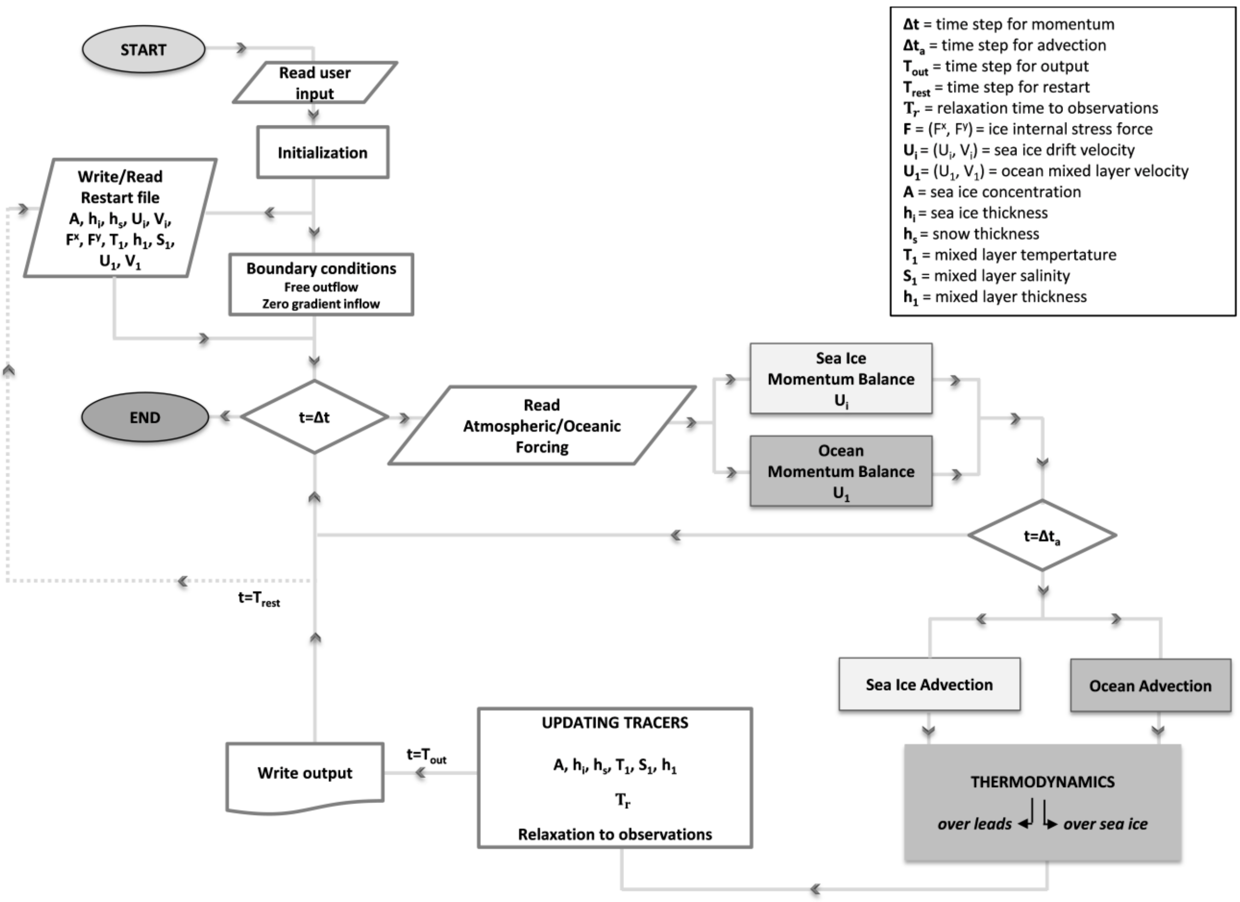

Fig. 4: Diagram flow of the coupled sea ice - ocean model.

2.3 Forcing Fields

The ocean forcing consists of climatological oceanographic profiles of ocean temperature and salinity developed through the analysis of available in situ temperature and salinity datasets. These datasets consist of hydrographic mooring and CTD profile data collected from February 1995 to January 2008 within the CLIMA (Climatic Long-term Interaction for the Mass-balance in Antarctica) project of the Italian National Research Antarctic Program (PNRA). The two climatological datasets include idealized monthly temperature and salinity values, spatially uniform in the model domain and varying vertically down to 800 meters in depth. In detail, 8 depth levels (0 m, -30 m, -50 m, -100 m, -150 m, -300 m, -500 m, -800 m) are chosen for the computation of climatological temperature and salinity profiles (see Section 2.3) that are subsequently used to calculate, by linear interpolation, the temperature, T_b, and salinity, S_b, at the base of the active layer as well as the restoring temperature, T_c, and salinity, S_c, in the active layer. As main atmospheric forcing, the Era-Interim reanalysis from the European Centre for Medium-Range Weather Forecasts (ECMWF), has been prescribed. The data extracted from the global domain provide surface six-hourly parameters at a 0.5 × 0.5 degree horizontal resolution covering the model domain with 16 × 11 grid points, in latitude × longitude. Specifically, the input data consist of the 10 meter eastward and northward wind components (m/s), the 2 meter temperature (K), the downward surface solar radiation (Wm^{-2} s), the surface (1000 mb level) pressure (Pa), the relative humidity (%), the total cloud cover (0-1) and the total precipitation accumulation (m of water). The oceanographic and atmospheric data have been spatially and temporally interpolated over the whole model domain. Meteorological observations form Automatic Weather Stations (AWSs) have also been employed to force the model.

2.3.1 Atmospheric field setting

The resolution of the local winds is a crucial factor in estimating sea ice and HSSW production, especially in a small coastal polynya like the TNB. In particular during winter, sea ice production in TNB is largely determined by katabatic winds which are the main control of the TNB polynya size (Petrelli et al., 2008; Gallé, 1997). Petrelli et al. (2008) showed that an insufficient resolution of the katabatic winds leads to an underestimation of sea ice winter production of up to 50%, which results in an underestimation of the formation rate of HSSW and consequently of AABW. On the other hand, low resolution winds reanalyses can also result in higher ice and AABW production because of an overestimated offshore component due to the coarse resolution orography (Stössel et al., 2011).

In spite of their relatively high resolution, the ECMWF reanalysis have been found to underestimate the wind speeds in several studies (Cullather et al., 1997; Fusco et al., 2002; Petrelli et al., 2008), providing therefore an improper representation of the wind fields along and offshore TNB. Also Mathiot et al. (2010) investigated the effect of the katabatic winds on sea ice and shelf water properties by correcting the ECMWF reanalyses winds with results from the MAR regional atmospheric model. To remedy this problem, we have applied a wind correction to coastal and offshore model grid points value combining the Era Interim data with in-situ atmospheric data from Automatic Weather Stations (AWSs), which show a significantly increased skill over ECMWF atmospheric variables (Petrelli et al., 2008).

A merging function has been designed so that the correction factor for each grid point value varies with the distance from the weather station. Era Interim and AWS data are merged resulting in the effective wind vector defined as

$$V_{eff} = V_{AWS}\, e^{-\frac{r}{R}} + V_{Era}\left(1 - e^{-\frac{r}{R}}\right), \qquad (21)$$

where V_{AWS} and V_{Era} are the wind vectors from AWS and ERA-Interim, respectively, r is the distance from the AWS and R is an e-folding length scale.

In particular, atmospheric data from two AWSs have been used. In a first phase of the sensitivity tests, only the Rita AWS (-74.72° S, 164.03° E), installed within the Meteo-Climatological Observatory of the PNRA in close proximity to the Italian base “Mario Zucchelli”, downstream of the Priestley Glacier (Fig. 3), has been considered.

Subsequently, the Manuela AWS (-74.95° S, 163.69° E), installed as part of the AWS project of the University of Wisconsin-Madison Antarctic Meteorology Program on Inexpressible Island, has been also included. The AWS Manuela lies downstream of the Reeves Glacier (Fig. 3), which represents one of the main routes for the katabatic flows from the interior of Antarctica.

The Rita and Manuela datasets consist, respectively, of one hourly and ten minute intervals data including air temperature (°C), wind speed (m/s) and direction (°N), surface pressure (hPa), and relative humidity (%). The merging function (21) has been applied also to the air temperature and relative humidity data.

Three experiments (Table 3) were carried out in order to examine the influence of the parameter R (see eq. 21) on the wind fields and, consequently, on sea ice and ocean currents in the TNB area. The model was run with the rheology parameter P^* =27500 × 10^4 N/m^2, as in Hibler and Walsh (1982), which is the most widely used value for the ice strength parameter. A demarcation ice collection thickness, H = 0.1 m and a relaxation time of $\mathrm{T}_r = 7$ days to climatological oceanic data were used. The time interval of the atmospheric input was set to 6 hours, while that of the output fields is such that the model gives a daily output for each computed variable.

The control experiment, referred to as CASE 1, uses R=25 km, the second experiment, CASE 2, uses a larger R=50 km, while CASE 3 differs from the control experiment in the absence of the merging between reanalyses and AWS data. The results of the simulations (Fig. 5a to c) show that an increasing of the parameter R (CASE 2) leads, as expected, to larger wind and ice drift and ocean velocities. The wind velocities have maximum values of 19.66 m/s in CASE 1 and 20.65 m/s in CASE 2, while in CASE 3, where the merging function is switched off, they reach a maximum value of only 7.27 m/s. Also sea ice and ocean current velocities, which reach values of 0.34 m/s and 0.06 m/s respectively in CASE 2, are significantly reduced in CASE 3.

Experiment	***R* (km)**
CASE 1	25
CASE 2	50
CASE 3	no merging

Table3: Case studies on the influence of the parameter *R* on wind fields.

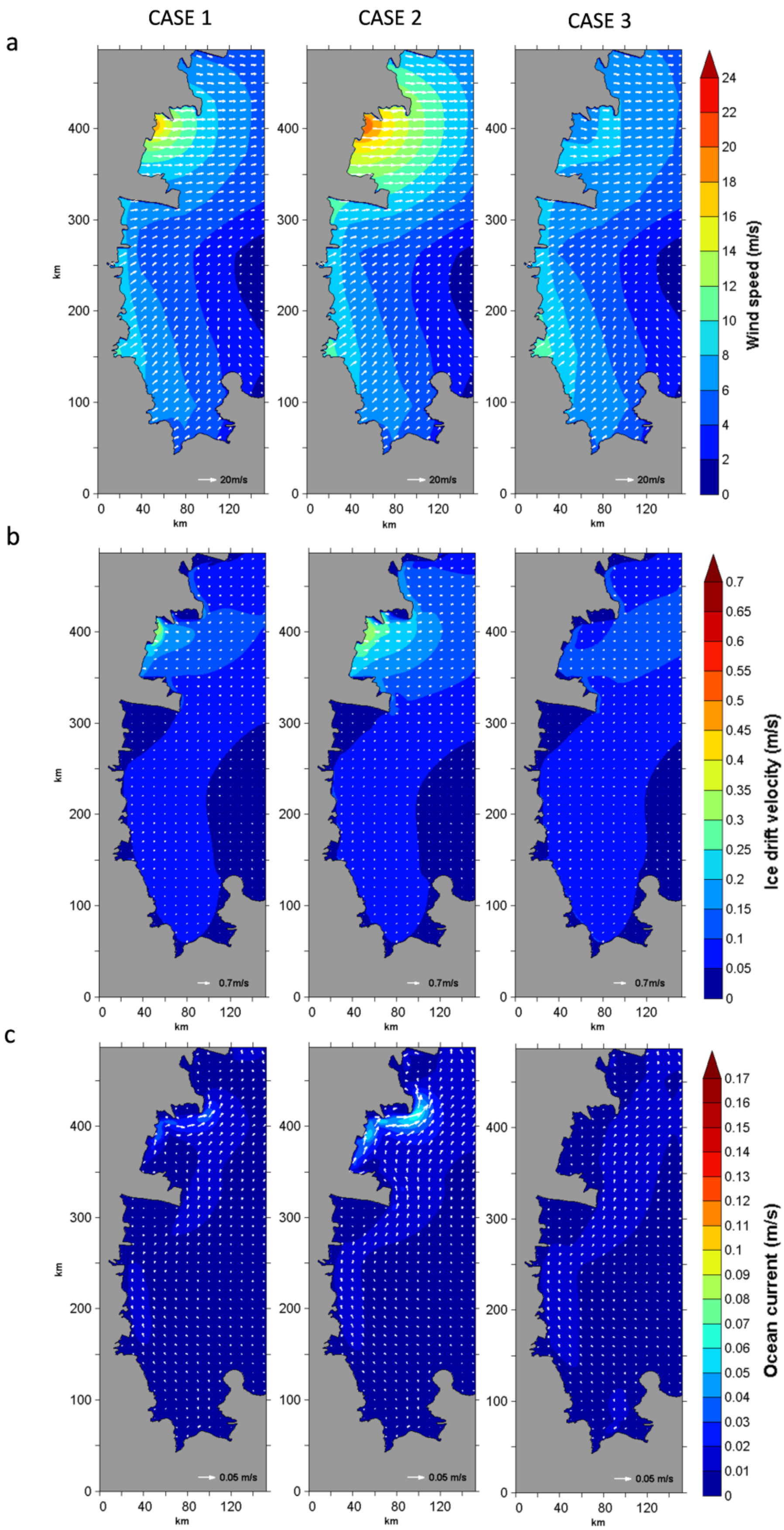

Fig. 5: Maps of wind speed (a), modelled ice drift velocity (b) and modelled ocean current (c) overlaid by the corresponding wind speed vectors, ice drift velocity vectors and ocean current vectors on 8th July 2000 for CASE 1 to CASE 3.

3. Sensitivity experiments

An improper choice of the parameters which describe sea ice evolution results often in unrealistic simulations leading to inaccurate results. Several sensitivity experiments were performed to define the best set of parameters controlling TNB sea ice dynamics and thermodynamics in response to wind forcing. Two key parameters have been found to control the wind driven polynyas: the rheological ice strength parameter $P*$ and the demarcation ice collection thickness H, also named the lead–closing parameter. The rate at which the leads close under freezing conditions is inversely proportional to the value of H. Both parameters have a strong effect on polynya size and sea ice extent and volume estimates (Hibler, 1979; Stössel et al., 1990; Stössel, 1992).

Finally a sensitivity analysis was carried out turning attention to the air-ice and ice-ocean drag coefficients which control the stresses on the sea ice cover. The choice of these parameters depends on the study area and especially on the wind forcing time and spatial resolution, therefore the model was opportunely tuned and optimized in this regard.

3.1 Sensitivity to ice strength parameter

The ice strength parameter $P*$ is a key element in sea ice rheology that relates sea ice strength (P) to its concentration, A, and mean thickness, Ah_i. It was first introduced by Hibler (1979) in the constitutive equation for sea ice strength as

$$\mathrm{P} = P^{*} A h_i \exp\left[-C(1-A)\right] \quad (22)$$

where $P*$ and C are empirical values. The ice strength exhibits a strong dependence on sea ice concentration and especially on the amount of thin ice. For a large amount of thin ice, the ice strength decreases significantly and most of thin ice is deformed (Hibler, 1979; Willmott et al., 2007; Feltham, 2008). Sea ice also offers less resistance to compression when Ah_i and $P*$ are low, and tends to pile up more easily because of enhanced mechanical ridging and rafting. Therefore, $P*$ is a critical parameter controlling sea ice drift behaviour in wind driven polynyas and represents the main tuning parameter to achieve a realistic sea ice drift pattern (Owens and Lemke, 1990; Stössel et al., 1990; Steele et al., 1997).

The strength of the ice internal forces depends on the state of deformation of the sea ice cover, which will, in turn be partly controlled by the wind stress field. Based on this observation, a sensitivity experiment was performed to investigate the impact on the ice dynamics of varying P^*. This experiment, referred to as CASE 4, is equal to CASE 1 shown in section 2.3.1 except for $P^* = 5000$ N/m^2 (Hibler, 1979). The wind field is the same as CASE 1 (see Fig. 5a) and the sea ice drift and ocean fields on 8th July 2000 for CASE 4 are shown in Fig. 6. These results are very similar to those of CASE 1 for both sea ice and ocean outputs.

The reduced ice strength does not affect significantly the ridging of sea ice or the sea ice drift in convergent regions, altering relatively little the ice concentration and thickness distribution (not shown). This indicates the polynya area is not highly sensitive to P^* in the determination of its opening/closure for this set of forcing.

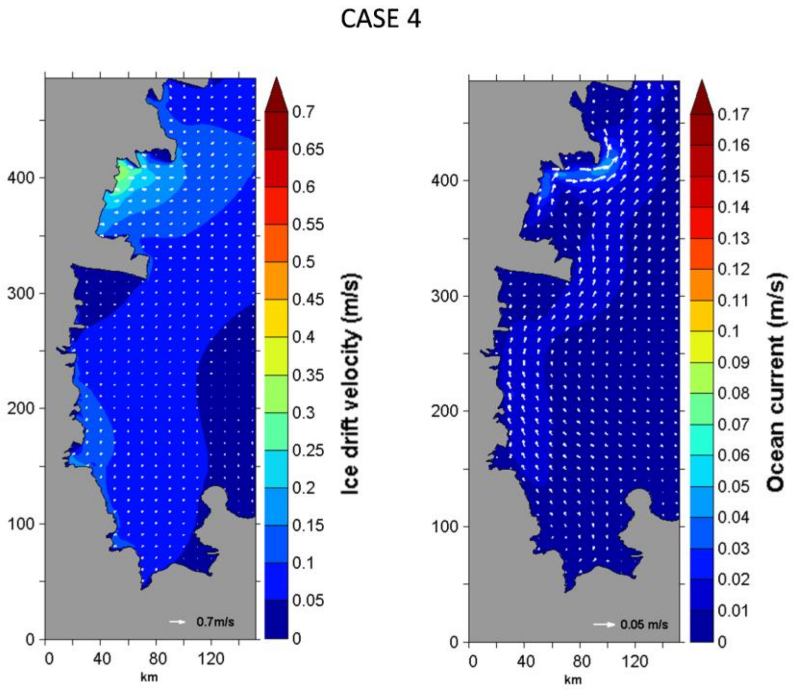

Fig. 6: Modelled ice drift velocity (left) and modelled ocean current (right) overlaid by the corresponding ice drift velocity vectors and ocean current vectors on 8th July 2000 for CASE 4.

This is probably due to the fact that this parameter has a major influence only in areas of thick ice but not so much in regions covered by thin and broken ice cover (Kreysher et al., 2000).

3.2 Sensitivity to demarcation ice collection thickness

While the dynamic behaviour of the consolidated ice is greatly determined by the ice rheology, the interior of the polynya is affected by the new ice thickness parameterization. The new ice thickness is controlled by the demarcation ice collection thickness parameter H in eq. (15) that is expressed as a transition value between thin ice (open water) and thick ice (Hibler, 1979). It is as crucial an element in sea ice models as the ice thickness collection depth in polynya flux models (Tear et al., 2003; Willmott et al., 2007) since it represents the thickness at which newly-formed ice in the polynya is transferred into thicker sea ice. Thereby, it affects sea ice thermodynamics, lowering heat loss through thin ice inside the polynya and determining primarily the mean thickness and sea ice concentration of newly formed ice (Hibler, 1979; Olason and Harms, 2010).

H has been often defined as a constant in the literature, with typical values in the range 0.1-0.5 m (Hibler, 1979; Pease, 1987; Ou, 1988; Darby et al. 1994, 1995). However, wind speed is an important controlling factor of the collection thickness of new ice (Mellor and Kantha, 1989; Winsor and Björk, 2000; Olason and Harms, 2010).

A number of experiments, outlined in Table 4, were performed with different values of H. The control experiment (CASE 5) was run with H=0.2 m, that is considered more appropriate than the H=0.5 m proposed by Hibler (1979), in simulating the behaviour of thin ice inside the polynya (Olason and Harms, 2010). In the second (CASE 6) and third experiment (CASE 7), sea ice concentration and thickness are simulated using a constant H=0.3 m and H=0.4 m respectively, while in the fourth experiment (CASE 8) a varying H has been used. Specifically, the collection depth parameterization of Winsor & Björk (2000) is employed, namely,

$$H = \frac{a + V \cdot b}{c}, \tag{23}$$

where V is the surface wind speed (m/s) and the constants are a = 1 m, b = 0.1 s and c = 15. This means that H varies in the range 0.1-0.3 m in the presence of wind speeds between 5-35 m/s.

In all these experiments, R is fixed to 50 km, except in CASE 9, in which the merging function is not applied. The value of 27500 N/m^2 for $P*$ and of 30 days for the relaxation time to oceanic forcing were used. Figure 7 shows the results of sea ice concentration (a) and thickness (b) simulation on 8th July 2000 for CASE 5–to–CASE 9. Note that a lower ice demarcation thickness gives higher ice concentration values and lower ice thickness values due to lower heat losses through leads.

Experiment	***H* (m)**
CASE 5	0.2
CASE 6	0.3
CASE 7	0.4
CASE 8	f (V)
CASE 9	0.2 no merging

Table 4: Sensitivity tests of sea ice evolution with respect to *H*.

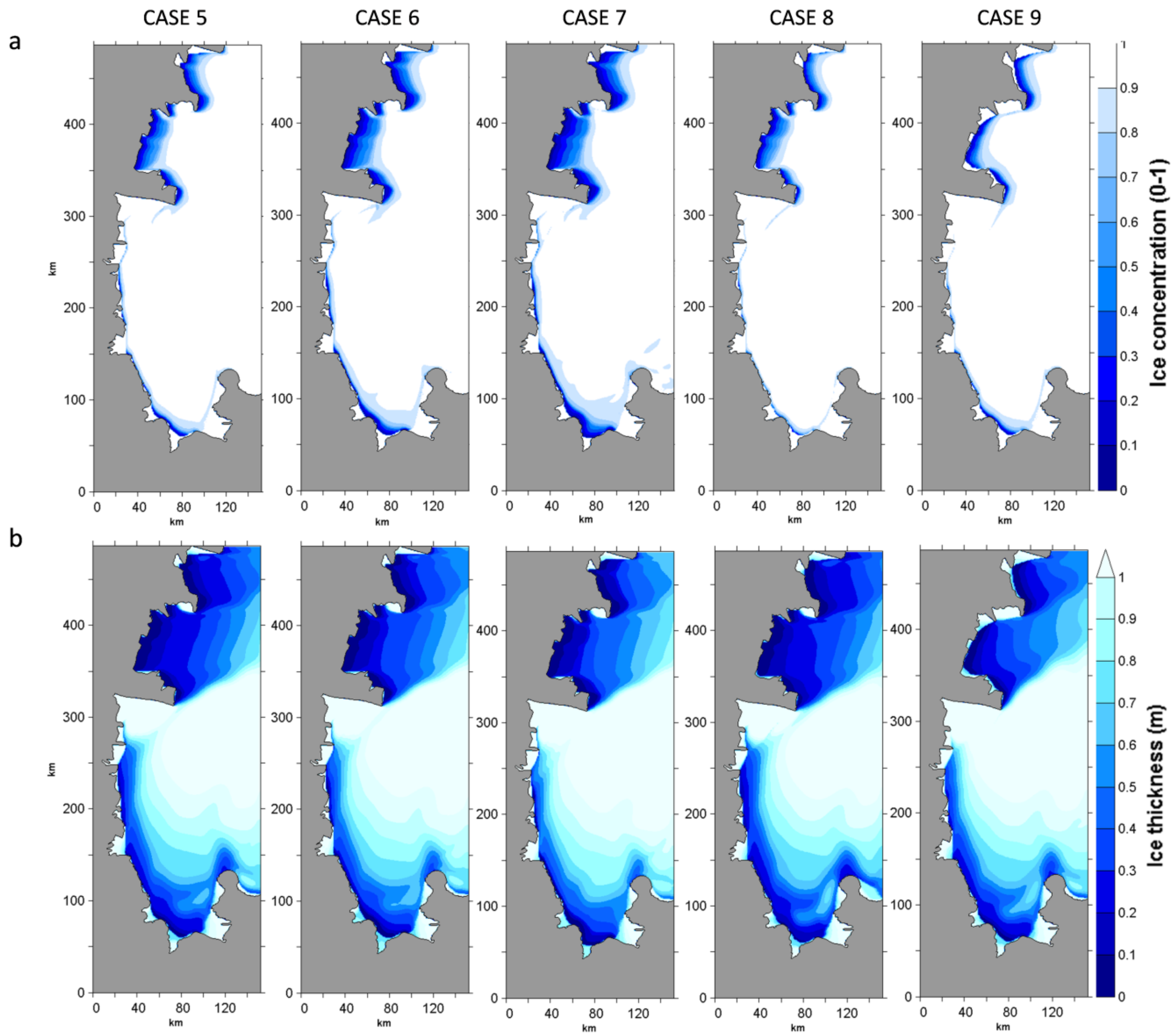

Fig. 7: Modelled sea ice concentration (a) and thickness (b) on 8th July 2000 for CASE 5 to CASE 9.

The sea ice distribution in CASE 8 is similar to that of CASE 5, suggesting that the dependence of the ice collection thickness on the wind velocities provides plausible values for *H*. This is well supported by the estimates of daily sea ice production (km^3/day) in TNB region on July 2000 (Fig. 8). Cumulative sea ice production (km^3) for the whole of July 2000 is also showed in Table 5. Note that the TNB region is identified by the area of the domain that extends within the ranges 1-120 km in X (longitude) and 310-425 km in Y (latitude) as shown in Fig. 8. Sea ice production rate computed using a non-spatially uniform *H* (CASE 8) depicted by the solid line with square markers shows a trend very similar to that of CASE 5, except for a few days when wind speeds in the polynya were particularly large. As it can easily be observed, CASE 9, where wind forcing is given by the winds reanalysis alone, underestimates considerably sea ice production rate compared to CASE 5 and, indeed, all the others. These results suggest reasonable agreement between the wind forcing and the simulated sea ice dynamics in the TNB.

In the next section we will consider the sensitivity of the TNB polynya to the wind forcing and wind stress (Stössel, 1992; Stössel et al., 2011) pointing out the importance of high temporal resolution of wind data.

Experiment	Sea ice production (km^3) in July 2000
CASE 5	10.08
CASE 6	11.09
CASE 7	12.12
CASE 8	9.79
CASE 9	6.83

Table 5: Sea ice production in July 2000 for the experiments CASE 5 to CASE 9.

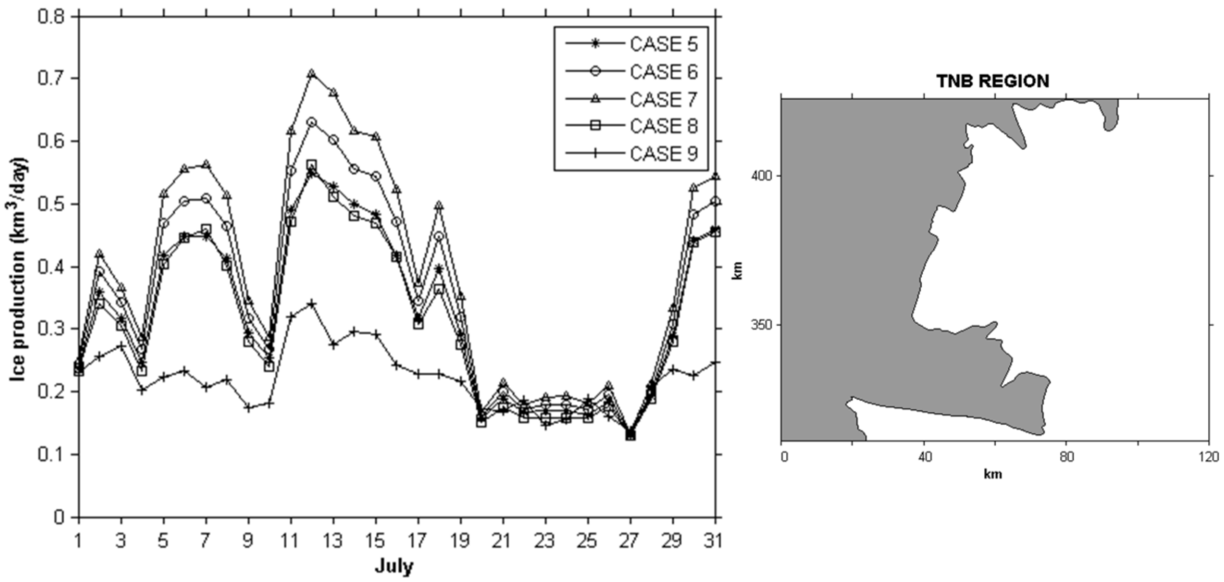

Fig. 8: Daily ice production (left) on July 2000 for CASE 5 to CASE 9 within a smaller area of the domain, defined as TNB region (right), extending approximately from 310 km to 425 km in Y and bordered by X = 120 km.

3.3 Sensitivity to air-ice and ice-ocean drag coefficients

Along with $P*$, the atmospheric and oceanic drag coefficients have been identified as crucial parameters for sea ice drift. Several sensitivity experiments were performed to obtain the optimal set of drag coefficients that would allow us to run the model under more realistic conditions.

We also focused on the regime of the katabatic winds and its impact on sea ice evolution in the TNB and on the polynya size. The latter, in fact, is very responsive to variations in the freezing rates in the bay as a result of a weakening of the katabatic flows or a change in their direction (Bromwich and Kurtz, 1984; Priestley, 1914). The duration of the katabatic wind events has a greater contribution than the intensity and frequency of the katabatic flows in determining the polynya extent (Ciappa et al., 2012; Rusciano et al., 2013). Rusciano et al. (2013) found most frequent katabatic events take place during the winter season and last on average from one to three hours. That means that long time intervals (daily/six hourly) atmospheric input probably misrepresent the real and local atmospheric fields in a given temporal period. On the other hand, a single source of AWS data fails to properly reproduce the geometry of the coastal wind regime resulting from the drainage of the interior katabatic airflows through the different confluence pathways (Petrelli et al., 2008). In view of these considerations, in the next experiments, the time resolution was increased so that the model is able to capture any katabatic events. Furthermore, a second dataset from AWS Manuela (see section 2.3.1) was taken into account to enlarge the area of influence of the katabatic flows. Unfortunately, no other weather station is available in the southernmost region of the bay and near to the Drygalski Ice Tongue. In addition, the merging function was modified and the range of influence of the AWS data on the reanalysis data was let to assume an elliptic shape rather than a circumference as follows:

$$V_{eff} = V_{AWS}\, e^{-\sqrt{\frac{x^2}{R_1^2}+\frac{y^2}{R_2^2}}} + V_{Era}\left(1 - e^{-\sqrt{\frac{x^2}{R_1^2}+\frac{y^2}{R_2^2}}}\right), \qquad (24)$$

where x and y are the components of the position vector of a particular point in the domain with respect to the AWS, and $R_1 = 50$ km and $R_2 = 20$ km are e-folding length scales in the x and y directions. Table 6 summarises the experiments performed to explore the impact of varying the C_{da} and C_{do} drag coefficients, increasing and/or decreasing the one with respect to the other, on sea ice drift and polynya dynamics. Substantially, an increasing of C_{da} and/or at the same time a decreasing of C_{do} allows sea ice to move faster and vice versa. We have made use of a double sub-index to identify easily the wind and ocean drag coefficients used in a particular experiment, e.g. the experiment denoted by E_{ab} uses $C_{da} = a \times 10^{-3}$ and $C_{do} = b \times 10^{-3}$.

The first experiment (E_{15}) is the control simulation of one winter month of the year 2005 for which the model has been configured with constant and more commonly used values for the drag coefficients, $C_{da} = 1 \times 10^{-3}$ and $C_{do} = 5 \times 10^{-3}$. In the next experiments, the values of the two drag coefficients were allowed to vary individually or simultaneously with respect to those of the control run. Specifically, in the second experiment (E_{35}) C_{da} varies and C_{do} is the same as in the control run, in the third experiment (E_{11}), only C_{do} varies, while, in the fourth (E_{31}) and in the fifth (E_{34}) experiments, both parameters vary together. The sixth experiment (E_r), which is in more detail described afterwards, was carried out using non constant values for the drag coefficients. All the experiments are forced with atmospheric forcing from the AWS Manuela at ten minutes resolution, combined with hourly data from the AWS Rita. The resulting values are averaged with the six hourly ERA-Interim data so as to adjust the background atmospheric fields, especially the winds. In addition, the output time of the variables simulated by the model were set equal to 3 hours since, as explained above, this value would appear to be a good compromise to capture the effects of katabatic winds.

As the sensitivity experiments described in previous sections, a significant dependence of the sea ice simulation on the wind forcing can be inferred from the results of the modelled output fields. The sea ice distribution appears to be very sensitive to the pattern of the wind stress which varies considerably depending on the surface winds. Fig. 9a shows the wind speeds and the wind stress vector fields for the E_{15}, E_{35}, E_{11}, E_{31} and E_{34}. The wind field is the same for all the experiments since they have been forced with the same wind configuration, which has maximum wind speed values of up to 23 m/s and a mean value of 9 m/s. The wind stress, depending on the drag parameters, exhibits average values of 0.16, 0.41, 0.13, 0.27 and 0.40 N/m^2 in E_{15}, E_{35}, E_{11}, E_{31}, E_{34}, respectively. The largest values have been found, as expected, in E_{35}, E_{31} and E_{34} with maxima of 1.48, 1.34 and 1.47 N/m^2 versus much smaller maxima in the CTRL run (E_{15}) and in E_{11} of approximately 0.54 N/m^2.

Experiment		C_{da}		C_{do}
E_{15}	<u>CTRL</u>	1×10^{-3}		5×10^{-3}
E_{35}		3×10^{-3}		5×10^{-3}
E_{11}		1×10^{-3}		1×10^{-3}
E_{31}		3×10^{-3}		1×10^{-3}
E_{34}		3×10^{-3}		4×10^{-3}
E_r		1×10^{-3} 3×10^{-3}	$V \leq 10$ m/s $V \geq 20$ m/s	$1.3 \times C_{da}$

Table 6: Sensitivity tests with respect to the air-ice and ice-ocean drag coefficients. The double sub-index identifies the wind and ocean drag coefficients used in each experiment.

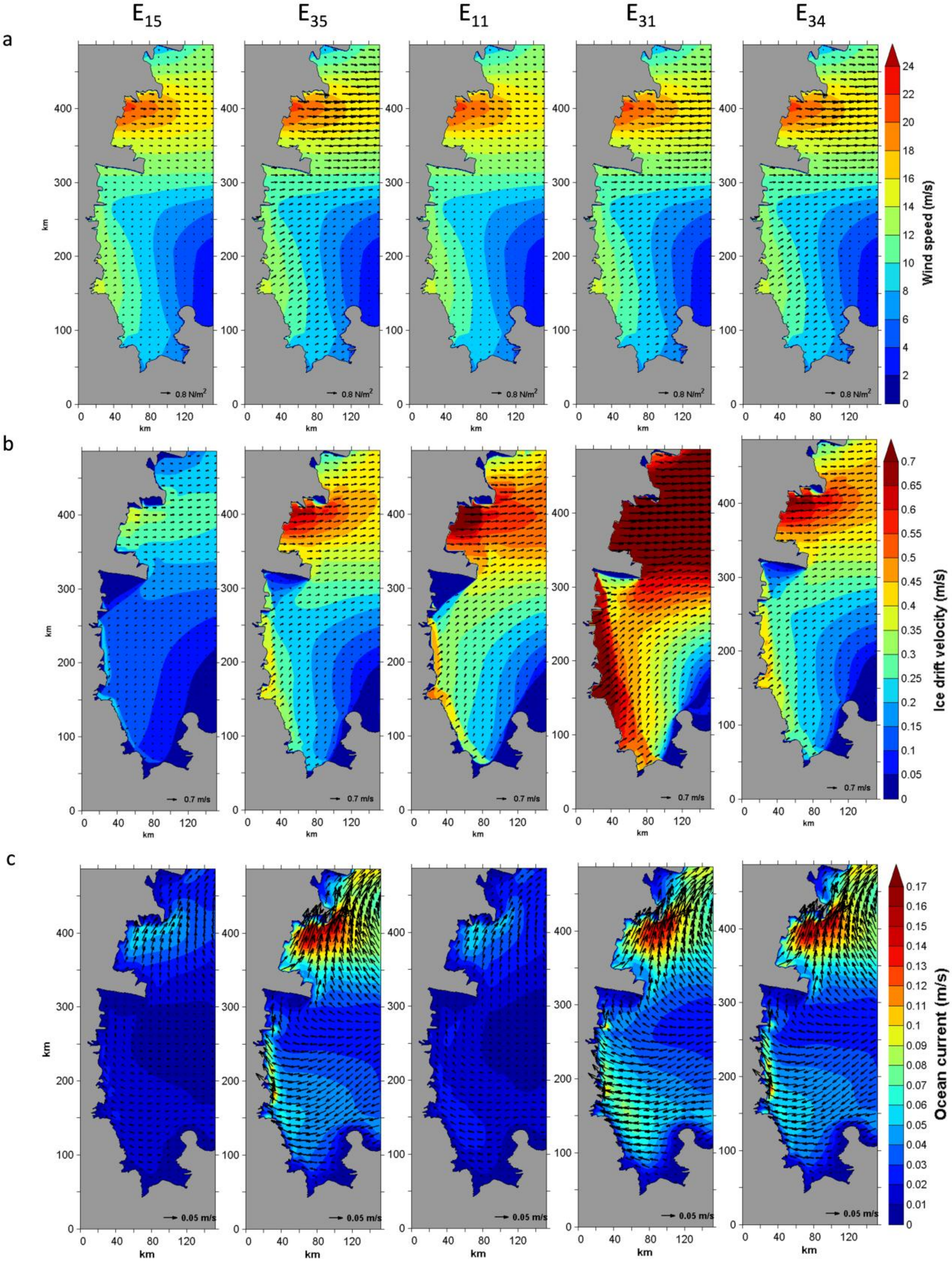

Fig. 9: Wind speeds (a), sea ice drift velocities (b) and ocean currents (c) with the superimposed wind stress, ice drift and ocean current vectors, respectively on 30th July 2005 for E_{15}, E_{35}, E_{11}, E_{31} and E_{34}.

The bigger wind stress in E_{35}, E_{31} and E_{34} leads to maximum ice drift speeds (Fig. 8b) of 0.65, 1.37 and 0.70 m/s respectively, and also to larger ocean currents (e. 8c). A maximum ice drift of 0.81 m/s, comparable to that from E_{34}, result from E_{11}, where the two coefficients C_{da} and C_{do} differ the least from each other. Smaller values, as expected, result from E_{15} with a maximum of 0.37 m/s and a mean of 0.12 m/s. Sea ice concentration and thickness charts displayed in Fig. 10a and b reveal that the sea ice distribution in E_{35}, E_{11} and E_{34} show a good comparison, from a qualitative point of view, with MODIS scenes represented in Ciappa et al. (2012). In these experiments the gap between C_{da} and C_{do} is small. In contrast, when C_{do} is much smaller than C_{da}, the ice drift becomes unrealistic and too strong also in regions out of the range of the coastal winds or, in the opposite case, really insignificant along shore. These results supports the importance of the C_{da}/C_{do} ratio considered to be the most basic dynamics parameter determining the mean drift speed (McPhee, 1980; Leppäranta, 1981; Stössel, 1992; Geiger et al., 1998; Harder and Fisher, 1999).

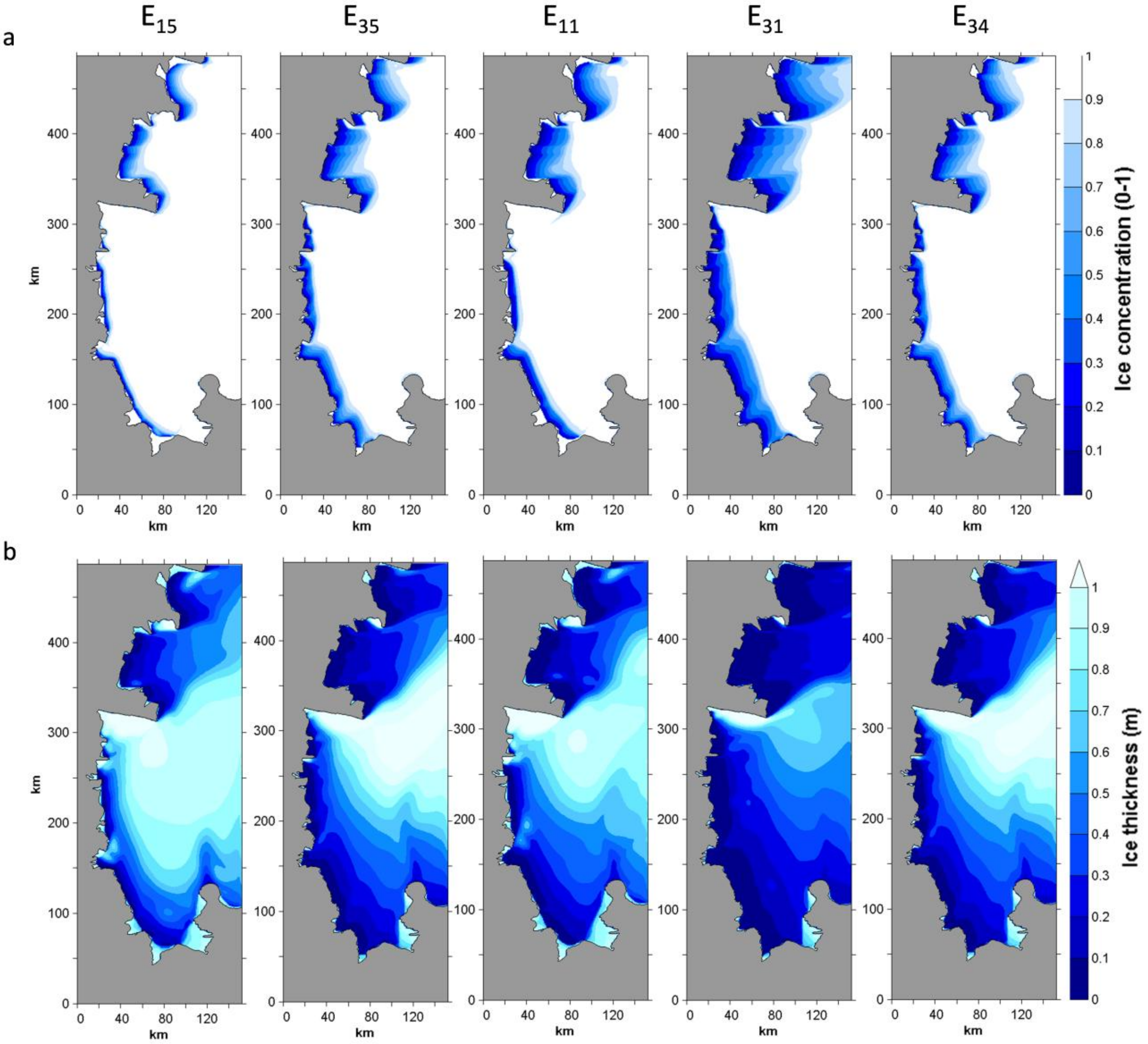

Fig. 10: Modelled sea ice concentration (a) and thickness (b) on 30th July 2005 for E_{15}, E_{35}, E_{11}, E_{31} and E_{34}.

Furthermore, unlike the strength parameter *P** which has a strong impact mainly on thick and more compact areas of the pack ice, the C_{da}/C_{do} ratio influences the ice drift in all regions during all seasons (Kreysher et al., 2000). The dependence of the air-ice drag coefficient on the wind speed has been also investigated by several authors (Large and Pond, 1981; Overland, 1985; Lynch et al., 1997). Accordingly, in the last experiment (E_r) C_{da} was allowed to vary linearly from 1×10^{-3} for wind speeds below 10 m/s, to 3×10^{-3} for wind speeds above 20 m/s. Then, C_{do} is allowed to depend linearly on the C_{da} through a constant factor of 1.3 (McPhee, 1980; Leppäranta, 1981; Stössel, 1992).

Figure 11 shows wind and ice velocities with the superimposed wind stress and ice velocity vector fields, ice concentration and thickness maps for E_r on the 30th July 2005 at 24:00. Mean and maximum values of the wind stress are very similar to those resulting from E_{34}. The results of E_r provide the best simulations of the sea ice dynamics of TNB.

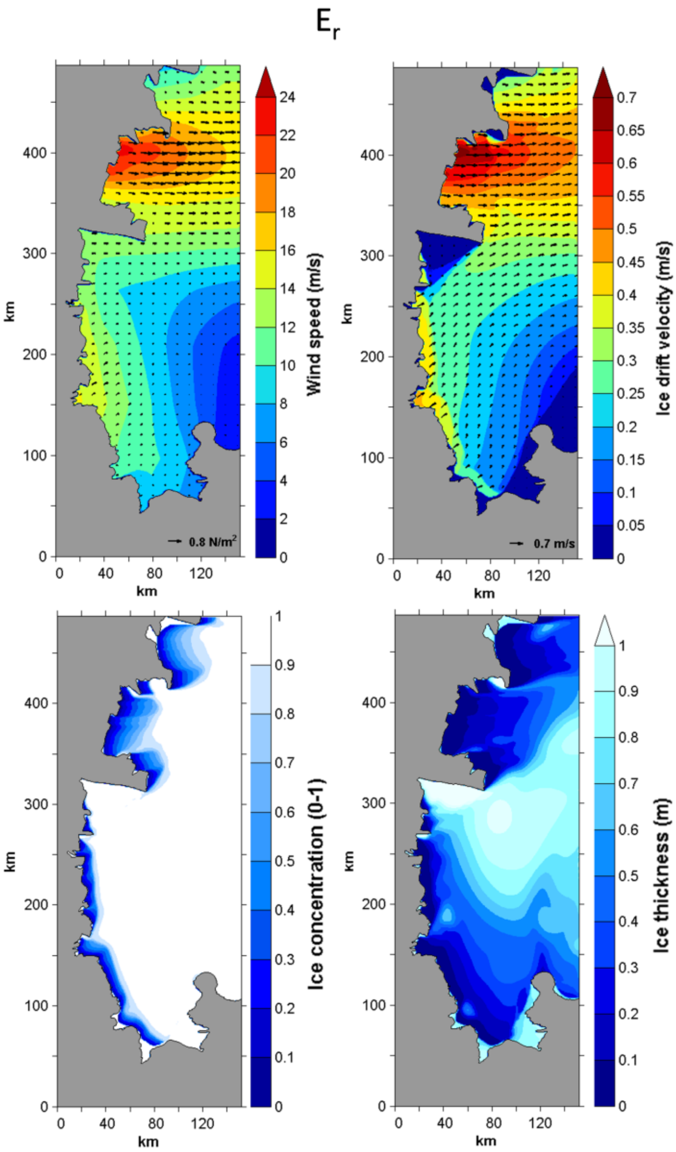

Fig. 11: Wind speeds and modelled sea ice drift velocities with the superimposed wind and ice drift vectors field (top) and sea ice concentration and thickness distribution (bottom) on 30th July 2005 for E_r.

4. One year numerical simulation and results

One year simulation of the TNB sea ice evolution has been carried out to investigate the polynya behaviour in response to the local katabatic flows. The main results of the 2005 simulation are discussed. The modelled polynya behaviour follows the characteristic dynamics of sea ice and ocean circulation in TNB. During the summer season, approximately from November to March, the bay is mostly ice free. It starts to be covered by sea ice in late March, when the low atmospheric and oceanic temperatures let the sea surface freeze. The evolution of the polynya is strongly controlled by the action of katabatic winds which allow TNB to be almost never completely ice covered in winter. Katabatic winds are very intense between April and October (Rusciano et al. 2013), and within this period several cycles of opening/closure of the polynya occurred.

Model-derived polynya extents in TNB region, defined in the section 3.2, have been computed for 2005. The polynya area is usually defined as the sum of the surfaces of open water and thin sea ice and therefore is restricted to the oceanic region within which the ice concentration is smaller than a given threshold (Willmott et al. 2007). This threshold is rather arbitrary, varying commonly from 0.5 to 0.7 (Parmiggiani 2006; Kern et al., 2007). An ice concentration threshold of 0.7 has been used here to estimate the TNB polynya extent (Fig. 12).

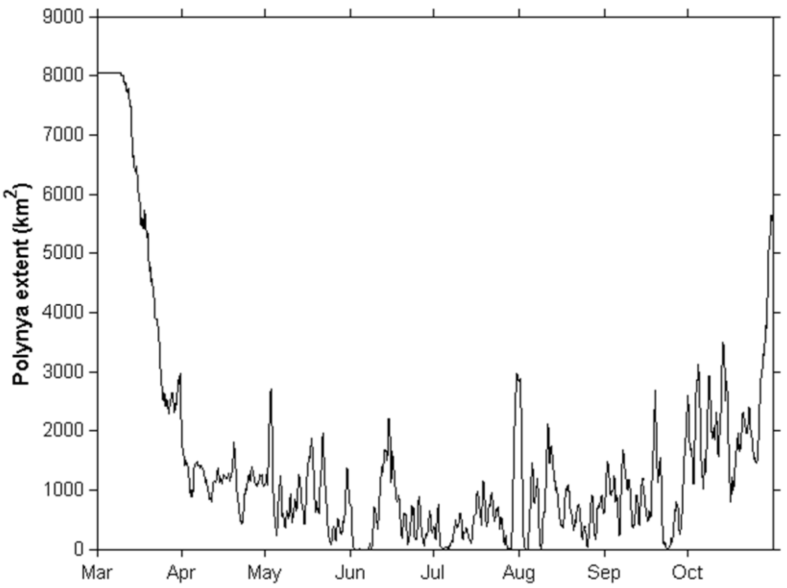

Fig. 12: Model-derived polynya extent in the TNB region from March to October 2005.

An increase of the polynya size is associated with the occurrence of katabatic events (not shown). The peak extent in midwinter occurred in July with a maximum value of 2962 km^2, followed by other two large extents of the polynya in August and September of 2868 km^2 and 2674 km^2 respectively (Table 7).

Polynya mean extents vary approximately from just over 500 km^2 up to almost 900 km^2, except in March/April, when sea ice formation processes start, and in October, which represents the end of the wintertime and the beginning of sea ice melting processes. The computed polynya extents are in good agreement with the wintertime values estimated by Petrelli et al. (2008) and with those recently published by Ciappa et al. (2012) who computed a mean annual open water of around 900 km^2 in the period 2005-2010 and 600 km^2 in 2006 using MODIS thermal infrared data. In any case, the computation of the polynya extent is not trivial since it depends on the accuracy and the limitations of the models and the remote sensing tools, as well as on their capability to resolve in time and in space the processes involved in the polynya variability. In addition, the local coastal winds have a strong but not exclusive impact on the polynya size which is caused by the interaction between katabatic forcing and synoptic weather conditions on longer timescales. The major effect of the katabatic winds on short timescales is the local recirculation of sea ice in TNB and its redistribution within the polynya area (Petrelli et al., 2008). The recirculation forced by these local winds enhances the ice production maintaining high ice production rates in open water and thin ice regions.

Winter months	Maximum Polynya extent (km^2)	Mean Polynya extent (km^2)
March	7946	5574
April	1806	1174
May	2688	871.2
June	2205	557.2
July	2962	532.5
August	2868	766.9
September	2674	875.6
October	5637	2304

Table 7: Monthly maximum and mean polynya extent of the TNB polynya from March to October 2005.

Sea ice production in the TNB region (Table 8) has been also computed by model sea ice fields outputs. The ice production rate, depends primarily on the presence of open water and on the surface wind speeds, therefore following the same trend as the TNB polynya extent. The spatial maximum sea ice production daily rate over TNB area exhibits a maximum of 0.70 km^3/day on 30th July that is equivalent to 48.08 cm/day. These estimates are comparable to those of Petrelli et al. (2008), who simulated the TNB polynya using a coupled atmosphere–sea ice model. She found in her high resolution experiment an ice production maximum daily rate of 26.4 cm/day during winter. Our results are quite consistent, even if slightly smaller, with ice production estimates obtained by Fusco et al. (2002) by applying a one-dimensional flux model to the TNB polynya. She computed for August 1993 and 1994 a maximum value of ice production of 85 cm/day and 72 cm/day respectively. Our daily ice productions result in a cumulative ice production value of 39.29 m over 2005 versus her yearly ice production of 81.7 m and 68.8 m for 1993 and 1994. However, these large values in Fusco et al. (2002) were obtained using AWS forcing, whereas the ice production was found to be significantly underestimated when computed by using the ECMWF data only. The spatially cumulative daily ice production is also showed in Fig. 13. The highest peaks of ice production occur in May, June and July with maxima of 0.61, 0.54 and 0.70 km^3 respectively. The cumulative ice production, that is the sea ice volume produced in the whole year 2005, is 57.91 km^3. This value is consistent with the estimation by Tamura et al. (2008) based on satellite data in combination with ERA-40 reanalysis data, which shows for the TNB polynya a mean annual cumulative sea ice production of 59.2$\pm$ 10 km^3. In particular, the ice volume created in the months of June and July amounts overall to 16.37 km^3, which is in good agreement with the value of 16.4 km^3 computed by Petrelli et al. (2008) in her winter experiment. The brine rejection, associated with the new ice production, and the HSSW production are also calculated. The brine rejection (kg/day) is parameterized as $P_S = \rho_i P_i (S_1 - S_i) \times 10^{-3}$ (see Markus et al., 1998; Van Woert, 1999a) where P_i is the ice production rate. The HSSW production (m^3/day) is computed following Van Woert (1999a) as $P_{HSSW} = P_S/\rho_{HSSW}(S_{HSSW} - S_{LSSW}) \times 10^{-3}$ where ρ_{HSSW} is the density of HSSW (1030.45 kg/m^3), S_{HSSW} is the salinity of HSSW (34.8) and S_{LSSW} is the salinity of Low Salinity Shelf Water or Warm Core Water (34.5) (Jacobs et al., 1985).

The salt and HSSW (Fig. 14) production are larger in wintertime, when the ice production is higher. Their cumulative values in the year 2005 within the TNB polynya are 1.7×10^{12} kg and 0.5×10^{13} m^3 respectively. These values are in good agreement with those of Fusco et al. (2002), Fusco et al. (2009) and Van Woert (1999a). Fusco et al. (2002), for example, estimated a salt production of about 4.6×10^{12} kg and a HSSW production of 1.5×10^{13} m^3 in the years 1993-94.

Winter months	Maximum daily rates of sea ice production (km^3/day)	Mean daily rates of sea ice production (km^3/day)	Monthly cumulative sea ice (km^3)
March	0.42	0.16	4.99
April	0.40	0.26	7.86
May	0.61	0.30	9.25
June	0.54	0.25	7.52
July	0.70	0.22	6.98
August	0.58	0.30	9.39
September	0.44	0.24	7.34
October	0.39	0.14	4.29

Table 8: Daily sea ice production rates from spatially cumulated ice production in TNB polynya region from March to October 2005.

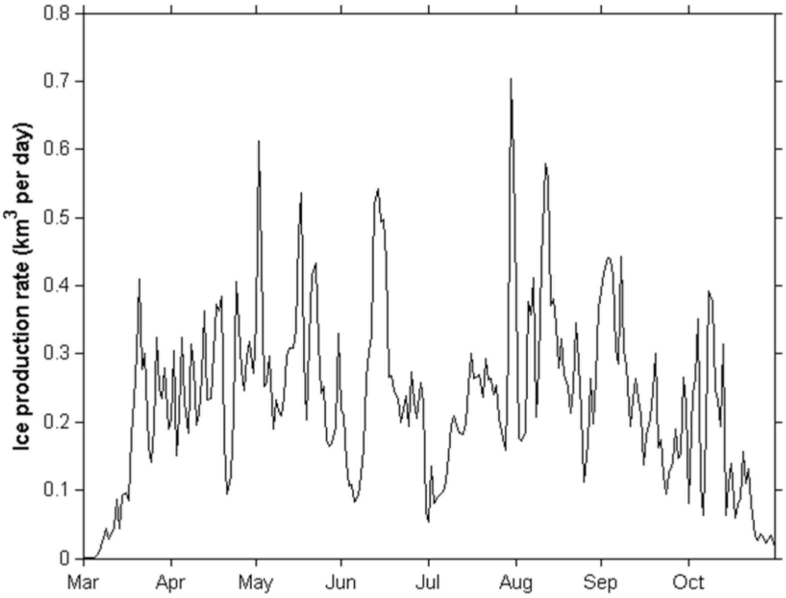

Fig. 13: Spatially cumulated daily rate of sea ice production in the TNB region from March to October 2005.

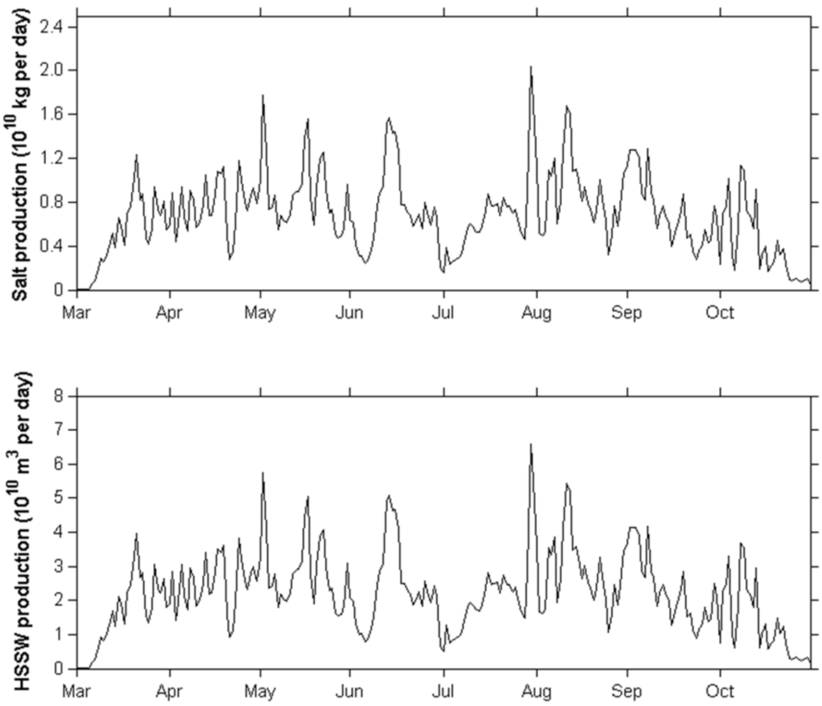

Fig. 14: Daily salt production (top) and HSSW production (bottom) in the TNB region from March to October 2005.

5. Model comparison with MODIS data

In situ measurements are particularly poor in remote or hardly accessible areas during the Antarctic winter, therefore satellite observations represent a useful tool in tuning sea ice-ocean models (Linch et al., 1997). Satellite images in combination with numerical weather prediction model data and in situ data from Automatic Weather Stations provide a good database to study polynya-atmosphere interactions in TNB area (Gallée, 1997; Ciappa et al., 2012).

Measurements of ice thickness and total ice volume in Terra Nova Bay do not exist. However, the model can be ground-truthed, at least in part, by comparing the polynya shape and extent to satellite images, which we do in the following. The NASA's MODIS (Moderate Resolution Imaging Spectroradiometer) sensor provides high temporal and spatial resolution measurements of Earth's land, ocean and atmospheric processes in several spectral bands and swath. The MODIS/Aqua Level 1B 1km Calibrated Radiances at 1 km resolution have been used to retrieve the ice surface temperature (IST) in the TNB region and subsequently to derive the polynya extent. Radiance data from MODIS channels 31 and 32 are converted to brightness temperatures (Kelvins) through the inversion of the Planck's law equation (Key et al., 1994). For ice/snow surface temperature (IST) computation the equation based on the technique of Key et al. (1997), originally developed for the Advanced Very High Resolution Radiometer (AVHRR), is used.

In order to investigate the dependence of the opening/closing cycles of the polynya on the wind forcing, a few significant periods in the wintertime of 2005 characterized by strong katabatic events have been identified. For each period, sea ice concentration charts from ice fields model outputs have been produced. The polynya edge is identified by the first contour line characterized by an ice concentration threshold of 0.7. These maps have been compared with MODIS IST images obtained following the aforementioned procedure for the same period. Figures 15 and 17 show the wind speed from both Rita and Manuela AWSs during two katabatic events observed in May and July

(1^{th} - 5^{th} May and 28^{th} - 31^{th} July respectively). The evolution of the polynya extent detected by MODIS can be seen in Figs. 16 and 18 where the modelled sea ice concentration for the same days is also showed. Sea ice concentration maps at the temporal steps closer to those of satellite scenes have been chosen to match at best model and MODIS products.

The model reproduces, reasonably well, sea ice concentration, depth and velocity as seen from the comparison with MODIS images. The drift of sea ice responds to wind forcing which shows a predominant West-West North West direction. Stronger winds are responsible for sea ice advection offshore, opening the polynya, and contributing to increasing its extent, while weaker winds just hamper the closure keeping the polynya opened. According to Pease (1987), a seaward wind component exceeding 10m/s is sufficient to maintain a polynya in coastal zones. Our results are in agreement with the suggested threshold.

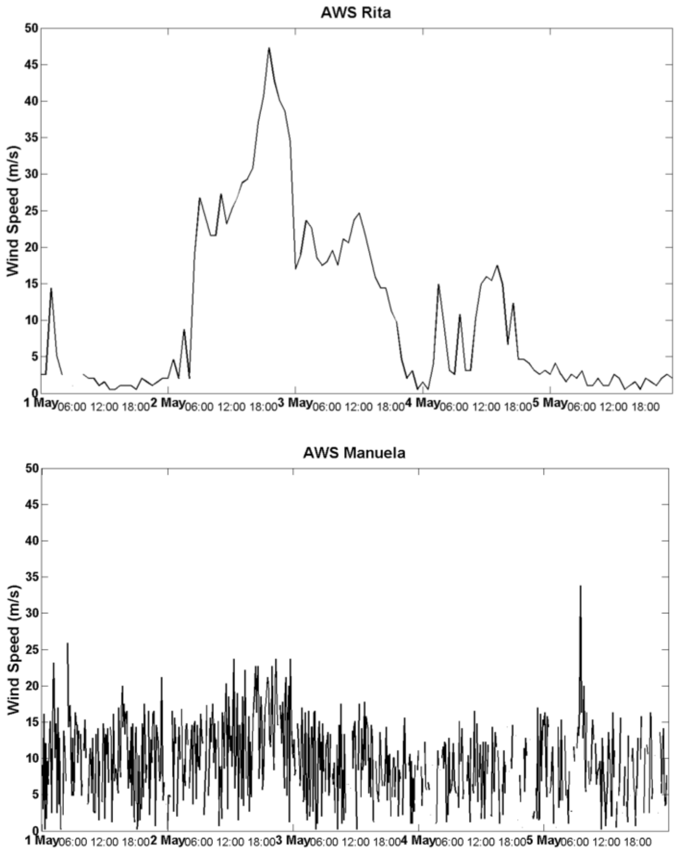

Fig. 15: Wind speed from Rita (top) and Manuela (bottom) AWSs on 1th-5th May 2005.

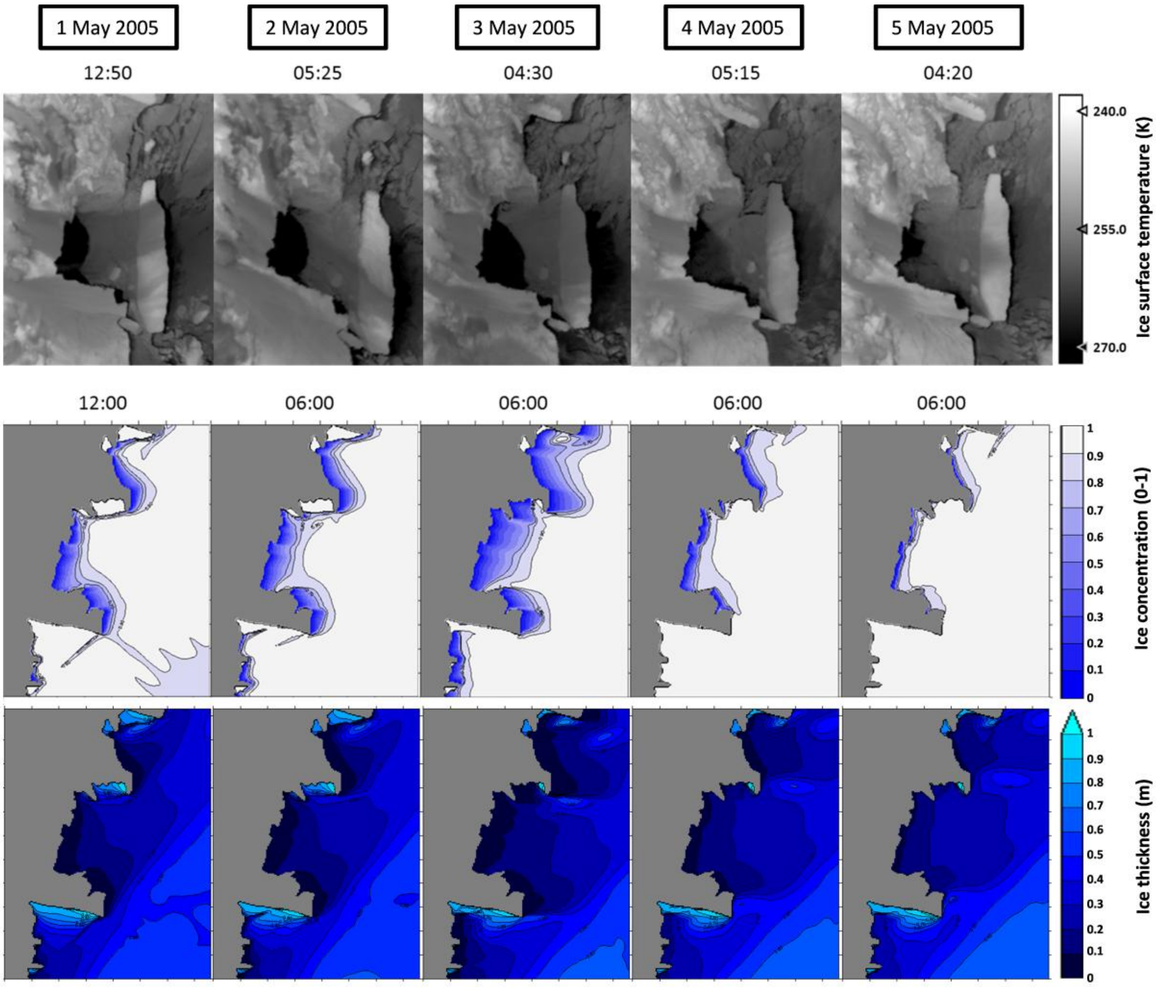

Fig. 16: IST MODIS scenes (top) and the modelled sea ice concentration and thickness maps (bottom) displaying the polynya evolution on 1th - 5th May 2005.

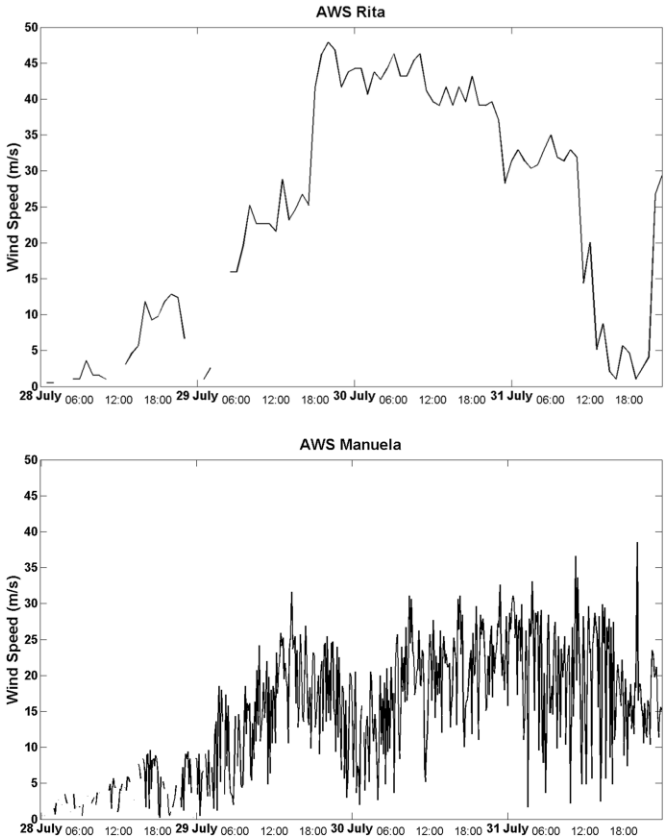

Fig. 17: Wind speed from Rita (top) and Manuela (bottom) AWSs on 28th - 31th July 2005.

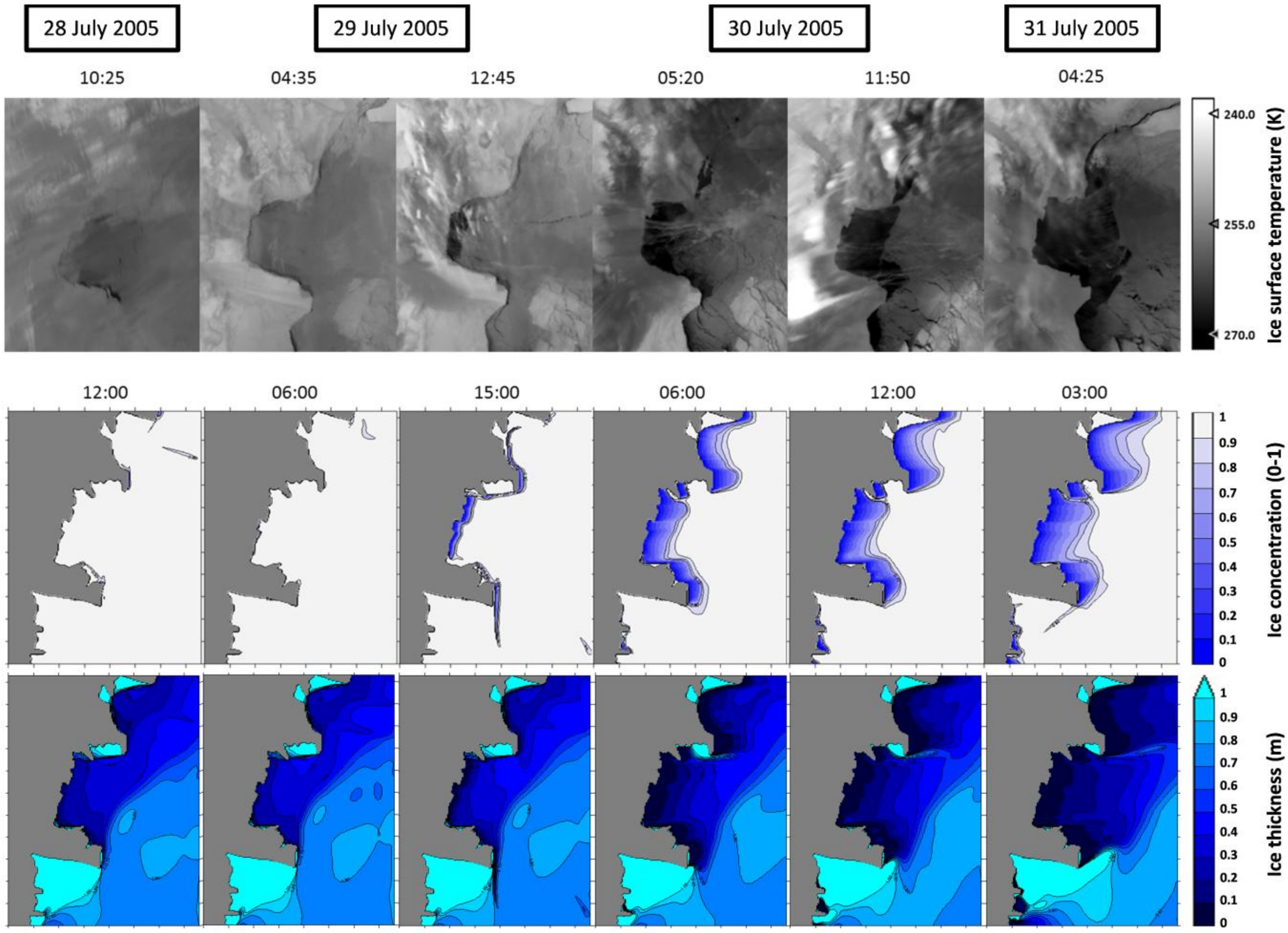

Fig. 18: IST MODIS scenes (top) and the modelled sea ice concentration and thickness maps (bottom) displaying the polynya evolution on 28th - 31th July 2005.

The small polynya observed at the beginning of the 1st of May (Fig. 16) increases its extent on the 2nd day of the month upon an increase of the wind speed measured by the AWS Rita, exhibiting a value well over 20 m/s and reaching a peak of almost 50 m/s. Wind speed from the AWS Manuela with an average value of 20 m/s contributes to enlarge the polynya eastward. The polynya size keeps on increasing at the beginning of 3rd of May until the wind speed drops sharply, below 10 m/s for AWS Rita, and the polynya starts closing on 4th and 5th of May. The discrepancies between the spatial distribution of sea ice in model simulations and IST MODIS scenes are thought to be partly due to the iceberg B-15A drifting in front of the TNB approximately in April-May 2005. The presence of this iceberg blocks the drift of sea ice offshore forcing the ice to accumulate in its proximity. In fact, in IST MODIS scenes the edge of the polynya is located more toward the coast and southward reducing thus the northern portion of the whole polynya extent. The simulation of sea ice distribution in July 2005 (Fig. 18) shows a higher degree of similarity with that observed in satellite images, probably because the advection of sea ice is less affected by the iceberg moving out of the bay. On 28th July the polynya is almost totally closed because the wind speeds are near to zero. After an enhancement of the wind forcing, the polynya starts opening at the beginning of the 29th of July and expands rapidly seaward. The largest opening of the polynya occurs on 31th July 2005 in response to the stronger wind speeds values recorded previously by AWS stations, near to 50 m/s for Rita and 40 m/s for Manuela. Some discrepancies between the simulated polynya and that observed in MODIS scenes may probably due to the gaps (missing data) in the AWSs wind datasets.

The TNB polynya extents have been also derived from both MODIS IST scenes and sea ice concentration maps on 28th -31th July. The aforementioned sea ice concentration threshold of 0.7 has been used for the modelled ice. A varying threshold for IST proposed by Ishikawa et al. (1996) and Zwally et al. (1983) that discriminates open water and thin ice from thick ice or land fast ice has been employed for satellite maps. Setting sea ice concentration to 0.7, our IST threshold is given by $T_{th} = 0.3T_f + 0.7T_{ice}$ where T_f is the temperature of the open water at the freezing point and T_{ice} is the temperature of sea ice around the polynya. Both temperature values are extracted from the IST scenes after they have been visually inspected one by one. In particular, T_f is given by the warmest IST found within the polynya and T_{ice} is estimated as the average of the IST values found around the open water.

Polynya extents from the 28th July to the 31th July are showed in Table 9. Polynya extent on the 31th July represents the largest opening of the whole of 2005, as also found in Ciappa et al. (2012). The model-derived polynya extents mostly agree with those computed from MODIS IST images, revealing the same temporal trend in polynya increasing during the observed katabatic event. The polynya extent values are less comparable to the MODIS based extents retrieved by Ciappa et al. (2012) showing a polynya extent of approximately 7615 km^2 on 31 July at 04:25 versus the corresponding MODIS-derived and model-derived polynya extents of 3393 km^2 and 2831 km^2, respectively. That is due to the wider domain considered in his estimates, including all the open water fraction occurred north of TNB (Wood Bay) and south of the Drygalski Ice Tongue.

TNB polynya event in July 2005	Model-derived polynya extent (km^2)	MODIS-derived polynya extent (km^2)
28th 12:00	12	40
29th 06:00	0	25
29th 15:00	389	391
30th 06:00	1858	1936
30th 12:00	2148	2385
31th 03:00	2831	3393

Table 9: TNB polynya extents from model sea ice concentration outputs and from MODIS IST from 28th to 31th July 2005.

6. Summary and concluding remarks

This work focuses on the investigation of sea ice formation in the TNB polynya in response to wind forcing. Because of the lack of direct observations related to sea ice fields, models provide valuable insight into the mean state of the ice cover (Flato, 2003) together with satellite observations which indeed fail often in availability and spatial resolution. A coupled sea ice-ocean model that simulates the seasonal cycle of sea ice formation and export within the polynya was presented. The model is applied to the TNB area, including also the nearby regions north and south of the bay in order to characterize at the best seasonal sea ice variability and polynya behaviour. The horizontal resolution is of 1 km, which is sufficient to represent the salient features of the coastline geometry, notably the Drygalski Ice Tongue. The model has been forced by a combination of Era Interim reanalysis by ECMWF and in-situ data from Rita and Manuela AWS, and also by in situ oceanic data.

The modelled sea ice fields have proved to be very sensitive to the atmospheric forcing. The sea ice evolution has been found to be shaped by different parameters involved in the dynamics of sea ice which in turn affects the thermal processes that occur in the ice cover. Several sensitivity experiments have been performed in order to optimize and set up a few main parameterizations and coefficients, thus improving the model outputs. The use of a demarcation ice collection thickness (H) varying with the wind speed used by Winsor & Björk (2000) seems to be the best choice, amongst the ones considered here, for simulating sea ice fields and thermodynamic heat losses through thin ice inside the polynya. In contrast, the rheology parameter P^* has not been found to affect significantly the drift of sea ice in this region, resulting in almost unchanged outputs of sea ice concentration and thickness distribution irrespective of the value used for P^*. The importance of the air drag coefficient, one of the most important factors in modelling ice motion, has been also stressed. First the responses of the model to constant values of the air-ice (C_{da}) and ice-ocean (C_{do}) drag coefficients and subsequently to the C_{da}/C_{do} ratio have been investigated, the latter being the most basic parameter of sea ice dynamics in determining the mean sea ice drift speed (Geiger et al., 1998; Harder and Fisher, 1999). A C_{da} varying with wind speed has been adopted, while C_{do} is forced to depend linearly on C_{da} through a constant factor. Also a wind enhancement function has been developed in order to try to improve the prediction of sea ice fields. However, its application was unsuccessful, causing unrealistically high large values of the wind stress.

A simulation of sea ice formation in TNB has been performed for the entire year 2005 to investigate the response of the polynya dynamics to wind forcing. Unsurprisingly, the largest openings of the polynya match the stronger katabatic winds which have been found in wintertime, mainly from April to October. The largest polynya opening occurs in July, with an extent of 2962 km^2, while the polynya extent over the wintertime 2005 ranges between approximately 500 km^2 and 900 km^2. Sea ice production and the associated brine and HSSW productions have also been computed, exhibiting values cumulated over 2005 of 57.91 km^3, 1.7×10^{12} kg and 0.5×10^{13} m^3, respectively. These results are in good agreement with those reported by Fusco et al. (2002, 2009) who estimated a salt production of about 4.6×10^{12} kg and a HSSW production of 1.5 ×10^{13} m^3 for the period 1993-1994.

In order to support and validate the model outputs, a comparison with sea ice conditions detected by satellite images has been thought essential. Satellite images from the MODIS sensor have been chosen for this purpose since they reach a high spatial resolution of 1 km, the same as that of the model. In order to explore the strong relationship between the wind field and the TNB polynya extent, some wintertime periods including significant katabatic events have been selected. For these periods the MODIS IST scenes have been compared with the modelled sea ice concentration maps. The TNB polynya area seems to be reproduced reasonably well by the model in terms of both shape and distribution of sea ice. However, differences in sea ice distribution respect to that observed in the MODIS IST scenes are visually detectable in some regions. These differences are most prominent in the areas located along the coast characterized by the variable shelf-ice borders and the presence of land fast ice. In particular, two areas, namely, the region south of Drygalski Ice Tongue and the region north of the TNB (Wood Bay) appear almost recurrently ice free in the modelled sea ice maps.

The TNB polynya extent has been also derived from MODIS IST scenes and the corresponding model sea ice maps from the 28th to 31th July 2005. The application of an ice state dependent threshold for IST in MODIS images let us to validate the polynya extent with higher reliability. The model-derived polynya extents are very similar to those computed from MODIS IST images.

Finally, despite the discrepancies in both sea ice distribution in some regions and polynya extents, the model performs well in reproducing sea ice evolution. These discrepancies will be investigated more extensively in the future through either an improvement of the model to capture land-fast ice or, more simply the use of a more accurate land mask including fast ice. The remote sensing detection of the polynya area and its extent is obviously affected by fog, clouds or other atmospheric disturbance that often compromise the quality of the used satellite images. At any rate, modelling the opening and closing polynya events is a difficult task especially if the size of polynya is relatively small, as is the case in Terra Nova Bay (Pease, 1987; Lynch et al., 1997; Petrelli et al., 2008). Our results have further highlighted the sensitivity of sea ice simulations to wind forcing, which is the major aspect stressed in numerous modelling works on Southern Ocean. Accurate sea ice simulations in terms of sea ice distribution and thickness can be achieved, provided that the model is forced with realistic winds and surface boundary conditions, in particular ocean temperatures, as found by Stössel et al. (2011). High resolution wind forcing is necessary to capture in more detail coastal sea ice processes, such as coastal polynyas, ice drift and ice compression against coastline features.

Acknowledgments

The authors are grateful to two reviewers for their constructive comments and suggestions, which have helped to improve the manuscript very significantly. The authors are thankful to the Meteo-Climatological Observatory of the Italian National Program for Research in Antarctica (PNRA) and the Antarctic Meteorological Research Center of the University of Wisconsin-Madison for the Automatic Weather Stations data sets. They are also grateful to the European Centre for Medium-range Weather Forecast for the interim reanalysis and to the MODIS Atmosphere and Archive and Distribution System Nasa Website for free access to MODIS radiance products. This work was performed in the framework of Coastal Ecosystem Functioning in a changing Antarctic ocean project (CEFA) of the PNRA.

References

Biggs N.R.T. and Willmott A.J., 2001: A steady-state coupled ocean-polynya flux model of the North Water, Baffin Bay, Geophys. Astrophy. Fluid Dyn,. 95, 1–29.

Bromwich D. H. 1989: An extraordinary katabatic wind regime at Terra Nova Bay, Antarctica, Mon Weather Rev., 117 (3), 688-695.

Budillon, G., Fusco, G., & Spezie, G., 2000: A study of surface heat fluxes in the Ross Sea (Antarctica). Antarctic Science, 12(2), 243–254.

Ciappa A., Pietranera L., and Budillon G., 2012: Observations of the Terra Nova Bay (Antarctica) polynya by MODIS ice surface temperature imagery from 2005 to 2010, Remote Sens. Environ., 119, 158–172.

Connolley W. M., Gregory J. M., Hunke E. C. and McLaren A. J., 2004: On the consistent scaling of terms in the sea ice dynamics equation. J. Phys. Oceanogr., 1776–1780.

Cullather R. I., Bromwich D. H. and Grumbine R.W., 1997: Validation of operational numerical analyses in Antarctic latitudes. J. Geophys. Res., 102, 13761-13784.

Darby M. S., Willmott A. J. and Mysak L. A., 1994: A nonlinear steady-state model of the North Water Polynya, Baffin Bay. Journal of Physical Oceanography, 24,1011-1020.

Darby M. S., Willmott A. J. and Somerville T. A., 1995: On the influence of coastline orientation on the steady state width of a latent heat polynya. J. Geophys. Res., 100, 13,625-13,633.

Gallée H., 1997: Air-sea interactions over Terra Nova Bay during winter simulation with a coupled atmosphere-polynya model, J. Geophys. Res., 102(D12), 13,835-13,849.

Geiger C. A., Hibler W. D. and Ackley S. F., 1998: Large-scale sea ice drift and deformation: Comparison between models and observations in the western Weddell Sea during 1992, J. Geophys. Res., 103(C10), 21,893-21,913.

Fichefet T. and Morales Maqueda M.A., 1999: Modelling the influence of snow accumulation and snow-ice formation on the seasonal cycle of the Antarctic sea-ice cover. Clim. Dyn., 15, 251–268.

Flato G. M., 2003: Sea Ice Modelling. Chapter 9 in Mass Balance of the Cryosphere: Observations and Modelling of Contemporary and Future Changes, eds. J. Bamber and A. Payne, Cambridge University Press, pg. 367-389.

Frezzotti, M., and M. C. G. Mabin, 1994: Twentieth century behavior of Drygalski Ice Tongue, Ross Sea, Antarctica, Ann. Glaciol., 20, 397–400.

Feltham, D.L. 2008. Sea ice rheology. Annu. Rev. Fluid Mech., 40, 91–112.

Fofonoff, P. and Millard, R.C. Jr, 1983: Algorithms for computation of fundamental properties of seawater, UNESCO Tech. Pap. in Mar. Sci., No. 44, 53 pp

Fusco G., Flocco D., Budillon G., Spezie G., Zambianchi E., 2002: Dynamics and Variability of Terra Nova Bay Polynya, Marine Ecology, 23, 201-209.

Fusco G., Budillon G., Spezie G., 2009: Surface heat fluxes and thermohaline variability in the Ross Sea and in Terra Nova Bay polynya, Cont. Shelf Res. 29, 1887-1895.

Gent P.R., McWilliams J.C., 1990: Isopycnal mixing in ocean circulation models. J. Phys. Oceanogr., 20, pp. 150–155

Harder, M. and Fischer H., 1999: Sea ice dynamics in the Weddell Sea simulated with an optimized model, J. Geophys. Res., 104, 11,151-11,162.

Hibler W. D. III, 1979: A dynamic thermodynamic sea ice model, J. Phys. Oceanog., 9, 815–846.

Hibler, W. D., III and Walsh J. E., 1982: On modeling the seasonal and interannual fluctuations of Arctic sea ice, J. Phys. Oceanogr., 12, 1514 – 1523.

Holland Paul R., Kwok R., 2012: Wind-driven trends in Antarctic sea-ice drift, Nature Geoscience 5, 872-875.

Hunke E. C. and J. K. Dukowicz 1997: An elastic-viscous-plastic model for sea ice dynamics, J. Phys. Oceanogr., 27, 1849-1868.

Ishikawa, T., Ukita, J., Ohshima, K. I., Wakatsuchi, M., Yamanouchi, T., & Ono, N., 1996: Coastal polynyas off East Queen Maud Land observed from NOAA AVHRR data, Journal of Oceanography, 52, 389–398.

Jacobs S. S. and Comiso J. C., 1997: Climate variability in the Amundsen and Bellingshausen Seas. J. Clim. 10, 697–709.

Jacobs S.S., Fairbanks R.G. and Horibe Y., 1985: Origin and evolution of water masses near the Antarctic continental margins: evidence from H2 18O/ H2 16O ratios in seawater, Antarct. Res. Ser., 43, 59-85.

Jacobs S. S. and Comiso J. C., 1989: Sea ice and oceanic processes on the Ross Sea continental shelf. J. Geophys. Res., 94, 18195-18211.

Jacobs S. S. and Comiso J. C., 1997: Climate variability in the Amundsen and Bellingshausen Seas. J. Clim. 10, 697–709.

Jacobs S.S., 2004: Bottom water production and its links with the thermohaline circulation, Antarct. Sci. 16 (4), 427–437.

Key J. R., Maslanik J. A., Papakyriakou T., Serreze M. C. and Schweiger A. J., 1994: On the Validation of Satellite-Derived Sea Ice Surface Temperature, Arctic, 47, 3, 280-287.

Key J. R., Collins J. B., Fowler C. and Stone R. S., 1997: High Latitude Surface Temperature Estimates From Thermal Satellite Data, Remote Sens. Environ., 61, 302-309.

Kern S., Spreen G., Kaleschke L., DE LA Rosa S., and Heygster G., 2007: Polynya Signature Simulation Method polynya area in comparison to AMSR-E 89 GHz sea-ice concentrations in the Ross Sea and off the Adélie Coast, Antarctica, for 2002–05: First results, Ann. Glaciol., 46, 409–418.

Kreysher M., Harder M., Lemke P. and Flato G. M., 2000: Results of the Sea-Ice Model Intercomparison Project: Evaluation of sea ice rheology schemes for use in climate simulations. J. Geophys. Res., 105(C5), 11,299–11,320.

Kurtz D. D. and Bromwich D. H., 1983: Satellite observed behavior of the Terra Nova Bay polynya. J. Geophys. Res., 88, 9717-9722.

Kurtz D. D. and Bromwich D. H., 1985: A recurring, atmospherically forced polynya in Terra Nova Bay. In Oceanology of the Antarctic Continental Shelf, Antarct. Res. Ser., 43, edited by S. S. Jacobs, 177-201, AGU, Washington, D.C.

Kwok R., Comiso J. C., Martin S. and Drucker R., 2007: Ross Sea polynyas: Response of ice concentration retrievals to large areas of thin ice. J. Geophys. Res., 112, C12012.

Large W., and Pond S., 1981: Open ocean momentum flux measurements in moderate to strong winds. J. Phys. Oceanogr., 11, 324–336.

Lefebvre W. and Goosse, H., 2005: Influence of the Southern Annular Mode on the sea ice-ocean system: The role of the thermal and mechanical forcing. Ocean Sci. 1, 145–157.

Lemke P., 1987: A Coupled One-Dimensional Sea Ice-Ocean Model, J. Geophys. Res., 92(C12), 13,164–13,172.

Leppäranta, M., 1981: On the structure and mechanics of pack ice in the Bothnian Bay, Finnish Mar. Res., 248, 3–86.

Liu J. P., Curry J. A. and Martinson D. G., 2004: Interpretation of recent Antarctic sea ice variability, Geophys. Res. Lett. 31, L02205.

Liu J. P. & Curry J. A., 2010: Accelerated warming of the Southern Ocean and its impacts on the hydrological cycle and sea ice, Proc. Natl Acad. Sci. USA 107, 14987–14992.

Lynch A. H., Glueck M. F., Chapman W. L., Bailey D. A. and J. E. Walsh, 1997: Satellite observation and climate system model simulation of the St. Lawrence Island Polynya, Tellus A, 49, 277-297.

Maksym, T., S.E. Stammerjohn, S. Ackley, and R. Massom. 2012. Antarctic sea ice—A polar opposite? Oceanography 25(3):140–151,

Markus, T., Kottmeier C. and Fahrbach E., 1998: Ice formation in coastal polynyas in the Weddell Sea and their impact on oceanic salinity, in Antarctic Sea Ice: Physical processes, interaction, and variability, Antarct. Res. Ser., vol. 74, edited by M. O. Jeffries, pp. 273 – 292, AGU, Washington, D. C..

Martinsen E. A. and Engedahl H., 1987. Implementation and testing of a lateral boundary scheme as an open-boundary condition in a barotropic ocean model. Coastal Eng. 11, 603–627.

Mathiot, P., Barnier B., Gallée H., Molines J. M., Le Sommer J., Juza M. and Penduff T., (2010): Introducing katabatic winds in global ERA40 fields to simulate their impacts on the Southern Ocean and sea-ice, Ocean Modell., 35, 146–160.

Maykut, G.A. 1978. Energy exchange over young sea ice in the central Arctic. J. Geophys. Res., 83(C7), 3646-3658.

McPhee, M. G., 1980: An analysis of pack ice drift in summer, in Sea Ice Processes and Models, edited by R. S. Pritchard, Univ. of Wash. Press, Seattle, 62-75.

Monterey G. and Levitus S., 1997: Seasonal Variability of Mixed Layer Depth for the World Ocean. NOAA Atlas NESDIS 14 U.S. Gov Printing Office, , Wash., D.C., 96 pp.

Mellor G. L. and Kantha L., 1989: An ice-ocean coupled model, J. Geophys. Res., 94, 10,937-10,954.

Morales Maqueda M. Á., Wilmott A. J. and Darby M. S., 1999: A numerical model for intercadal variability of sea ice cover in the Greenland-Iceland-Norwegian Sea, Climate Dynamics, 15(2), 89-113.

Morales Maqueda M. Á., Willmott A. J., Biggs N. R. T., 2004: Polynya Dynamics: A review of observations and modelling, Reviews of Geophysics, 42, RG1004.

Mellor G. L. and Kantha L., 1989: An ice-ocean coupled model, J. Geophys. Res., 94, 10,937-10,954.

Olason E. O., and Harms I., 2010: Polynyas in a dynamic-thermodynamic sea-ice model, The Cryophere, 4, 147-160.

Orsi A. H., Johnson G. C. and Bullister J. L., 1999: Circulation, mixing and production of Antarctic bottom water, Progress in Oceanography, 43, Pergamon, 55–109.

Ou H. W., 1988: A time-dependent model of a coastal polynya, J. Phys. Oceanogr., 18, 584–590.

Overland J. E., 1985: Atmospheric boundary layer structure and drag coefficients over sea ice, J. Geophys. Res., 90, 9029-9049.

Owens W. B., Lemke P., 1990: Sensitivity studies with a sea ice-mixed layer-pycnocline model in the Weddell Sea. J. Geophys. Res., 95, C6, 9527-9538.

Pacanowski R. and Philander S.G.H., 1981: Parameterization of vertical mixing in numerical models of tropical oceans, J. Geophys. Res. 11, 1443–1451.

Parkinson C. L. and Cavalieri D. J., 2012: Antarctic sea ice variability and trends, 1979-2010, The Cryosphere, 6, 871–880.

Parmiggiani, F. 2006: Fluctuations of Terra Nova Bay polynya as observed by active (ASAR) and passive (AMSR-E) microwave radiometers, Int. J. Remote Sensing, 27(12), 2459–2467.

Pease C. H., 1987: The size of wind-driven coastal polynyas, J. Geophys. Res., 92, 7049–7059.

Petrelli P., Bindoff N. L. and Bergamasco A., 2008: The sea ice dynamics of Terra Nova Bay and Ross Ice Shelf Polynyas during a spring and winter simulation, J. Geophys. Res., 113.

Rothrock D. A., 1979: Modeling sea-ice features and processes, Journal of Glaciology, 24, 90.

Rusciano E., Budillon G., Fusco G., and Spezie G., 2013: Evidence of atmosphere-sea ice-ocean coupling in the Terra Nova Bay polynya (Ross Sea-Antarctica), Continental Shelf Research 61-62, 112-124.

Russell J.L., Stouffer R.J., and Dixon K.W., 2006: Intercomparison of the Southern Ocean circulations in IPCC coupled model control simulations, J. Clim. 19:4,560–4,575.

Semtner A. J., 1976: A model for the thermodynamic growth of sea ice in numerical investigations of climate, J. Phys. Oceanogr., 6, 27–37.

Steele, M., J. Zhang, D. Rothrock and H. Stern. 1997. The force balance of sea ice in a numerical model of the Arctic Ocean. J. Geophys. Res., 102(C9), 21,061–21,079.

Stössel A., Lemke P. and Owens W.B., 1990: Coupled sea ice-mixed layer simulations for the Southern Ocean, J. Geophys. Res., 95, 9539-9555.

Stössel A., 1992: Sensitivity of the Southern Ocean sea-ice simulations to different atmospheric forcing algorithms, Tellus A, 395-413.

Stössel A., Zhang Z., and Vihma T., 2011: The effect of alternative real-time wind forcing on Southern Ocean sea-ice simulations, J. Geophys. Res., 116, C11021.

Tamura T., Ohshima Kay I. and Nihashi S., 2008: Mapping of sea ice production for Antarctic coastal polynyas, J. Geophys. Lett., 35.

Tear S., Willmott A.J., Biggs N.R.T., Morales Maqueda M.A., 2003: One-dimensional models for the closure of a coastal latent heat polynya, J. Phys. Oceanogr. 33, 329–342.

Trumbore S.E., Jacobs S. S. and Smethie JR W. M., 1991: Chlorofuorocarbon evidence for rapid ventilation of the Ross Sea. Deep-Sea Research, 38, 845-870.

Turner J., Comiso J. C., Marshall G. J., Lachlan-Cope T. A., Bracegirdle T., Maksym T., Meredith M. P., Wang Z., and Orr A., 2009: Non-annular atmospheric circulation change induced by stratospheric ozone depletion and its role in the recent increase of Antarctic sea ice extent, Geophys. Res. Lett., 36, L08502.

Van Woert M. L., 1999a: The wintertime expansion and contraction of the Terra Nova Bay polynya. In Oceanography of the Ross Sea: Antarctica, edited by G. Spezie and G. M. R. Manzella, pp. 145-164, Springer-Verlag, New York.

Van Woert M. L., 1999b: Wintertime dynamics of the Terra Nova Bay polynya. J. Geophys. Res., 104, 7753-7769.

Willmott A. J., Holland D. M. and Morales Maqueda, M. A., 2007: Polynya modelling. In: Smith, Walker, O.; Barber, David, G., (eds.) Polynyas: windows to the world. Amsterdam, Elsevier, 87-125. (Elsevier Oceanography Series, 74).

Winsor P. and Björk G., 2000: Polynya activity in the Arctic Ocean from 1958 to 1997, J. Geophys. Res., Oceans 105, 8789-8803.

Zhang J, 2007: Increasing Antarctic Sea Ice under Warming Atmospheric and Oceanic Conditions, *J. Climate*, 20, 2515–2529.

Zwally H. J., Comiso J. C., Parkinson C. L., Campbell W. J., Carsey F. D., and Gloersen P., 1983: Antarctic Sea Ice, 1973–1976: Satellite Passive-Microwave Observations,Washington, DC, National Aeronautics and Space Administration, 206 pp.

Figure and table captions

Fig. 1: Overview map of TNB (Western Ross Sea) showing the major geographical features of this region and its surroundings (Kurtz and Bromwich, 1983).

Fig. 2: Schematic view of the main variables of the coupled sea ice – ocean model. The radiative and turbulent heat fluxes are separately calculated over the ice free (leads) and ice covered areas.

Fig. 3: The model domain showing the Drygalski Ice Tongue (DIT) and the two preferential paths of the katabatic flows, the Priestley and the Reeves Glaciers. The italian base, Mario Zucchelli Station (MZS), and the location of the automatic weather stations, Rita (AWS-R: 74.72°S, 164.03°E) and Manuela (AWS-M: 74.95°S, 163.69°E) are also indicated.

Fig. 4: Diagram flow of the coupled sea ice - ocean model.

Fig. 5: Maps of wind speed (a), modelled ice drift velocity (b) and modelled ocean current (c) overlaid by the corresponding wind speed vectors, ice drift velocity vectors and ocean current vectors on 8th July 2000 for CASE 1 to CASE 3.

Fig. 6: Modelled ice drift velocity (left) and modelled ocean current (right) overlaid by the corresponding ice drift velocity vectors and ocean current vectors on 8th July 2000 for CASE 4.

Fig. 7: Modelled sea ice concentration (a) and thickness (b) on 8th July 2000 for CASE 5 to CASE 9. The color version of this figure is available online.

Fig. 8: Daily ice production (left) on July 2000 for CASE 5 to CASE 9 within a smaller area of the domain, defined as TNB region (right), extending approximately from 310 km to 425 km in Y and bordered by X = 120 km.

Fig. 9: Wind speeds (a), sea ice drift velocities (b) and ocean currents (c) with the superimposed wind stress, ice drift and ocean current vectors, respectively on 30th July 2005 for E_{15}, E_{35}, E_{11}, E_{31} and E_{34}.

Fig. 10: Modelled sea ice concentration (a) and thickness (b) on 30th July 2005 for E_{15}, E_{35}, E_{11}, E_{31} and E_{34}. The color version of this figure is available online.

Fig. 11: Wind speeds and modelled sea ice drift velocities with the superimposed wind and ice drift vectors field (top) and sea ice concentration and thickness distribution (bottom) on 30th July 2005 for E_r.

Fig. 12: Model-derived polynya extent in the TNB region from March to October 2005.

Fig. 13: Spatially cumulated daily rate of sea ice production in the TNB region from March to October 2005.

Fig. 14: Daily salt production (top) and HSSW production (bottom) in the TNB region from March to October 2005.

Fig. 15: Wind speed from Rita (top) and Manuela (bottom) AWSs on 1th - 5th May 2005.

Fig. 16: IST MODIS scenes (top) and the modelled sea ice concentration and thickness maps (bottom) displaying the polynya evolution on 1th - 5th May 2005. The color version of this figure is available online.

Fig. 17: Wind speed from Rita (top) and Manuela (bottom) AWSs on 28th - 31th July 2005**.**

Fig. 18: IST MODIS scenes (top) and the modelled sea ice concentration and thickness maps (bottom) displaying the polynya evolution on 28th - 31th July 2005. The color version of this figure is available online.

Table 1: Input parameters of the model. The "x" stands for a varying value assigned to that parameter in the sensitivity experiments.

Table 2: Physical parameters of atmosphere, sea ice and ocean.

Table3: Case studies on the influence of the parameter *R* on wind fields.

Table 4: Sensitivity tests of sea ice evolution with respect to *H*.

Table 5: Sea ice production in July 2000 for the experiments CASE 5 to CASE 9.

Table 6: Sensitivity tests with respect to the air-ice and ice-ocean drag coefficients. The double sub-index identifies the wind and ocean drag coefficients used in each experiment.

Table 7: Monthly maximum and mean polynya extent of the TNB polynya from March to October 2005.

Table 8: Daily sea ice production rates from spatially cumulated ice production in TNB polynya region from March to October 2005.

Table 9: TNB polynya extents from model sea ice concentration outputs and from MODIS IST from 28th to 31th July 2005.

Figure(s)
Click here to download high resolution image

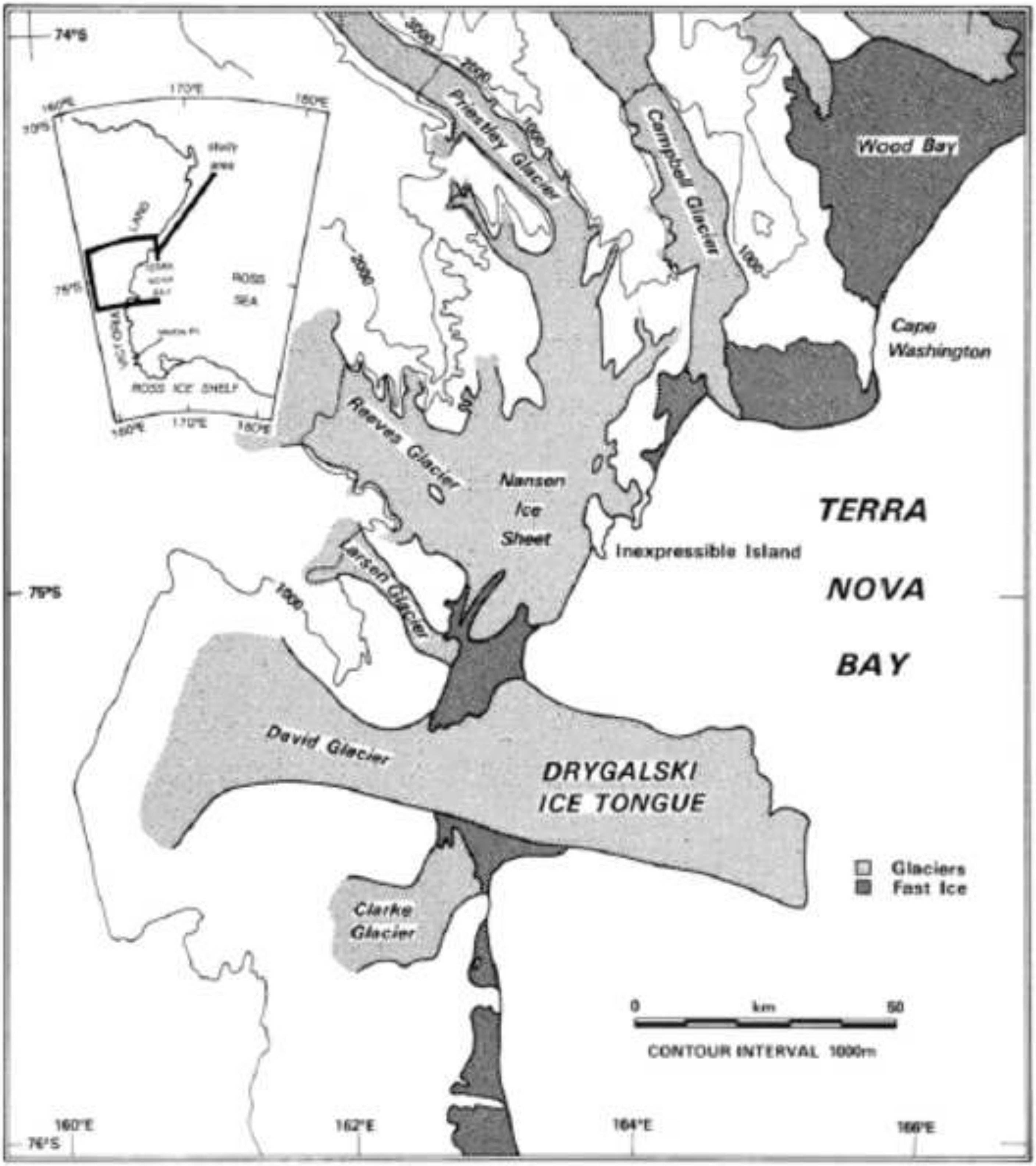

Figure(s)
Click here to download high resolution image

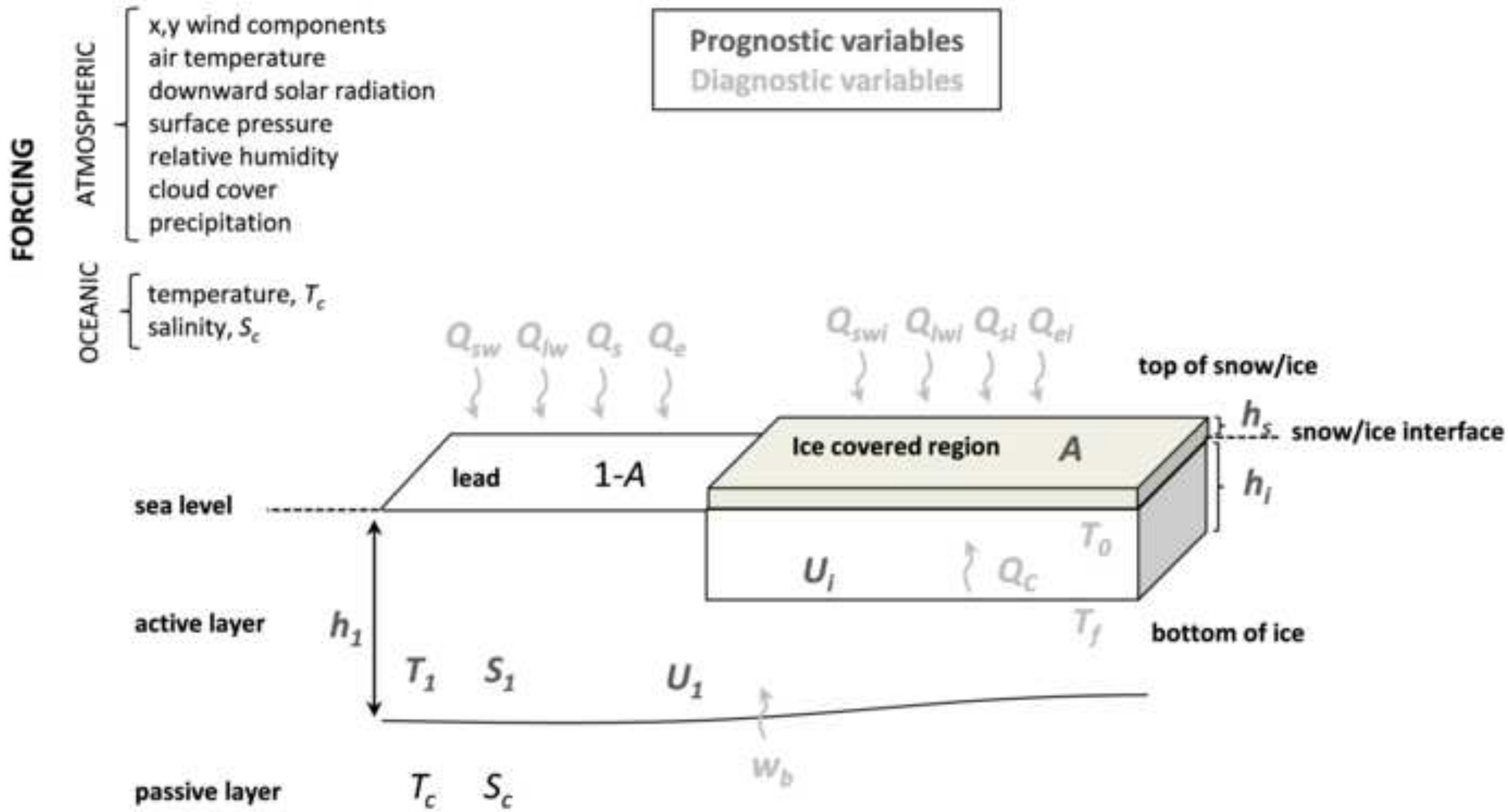

Figure(s)
Click here to download high resolution image

Figure(s)

Click here to download high resolution image

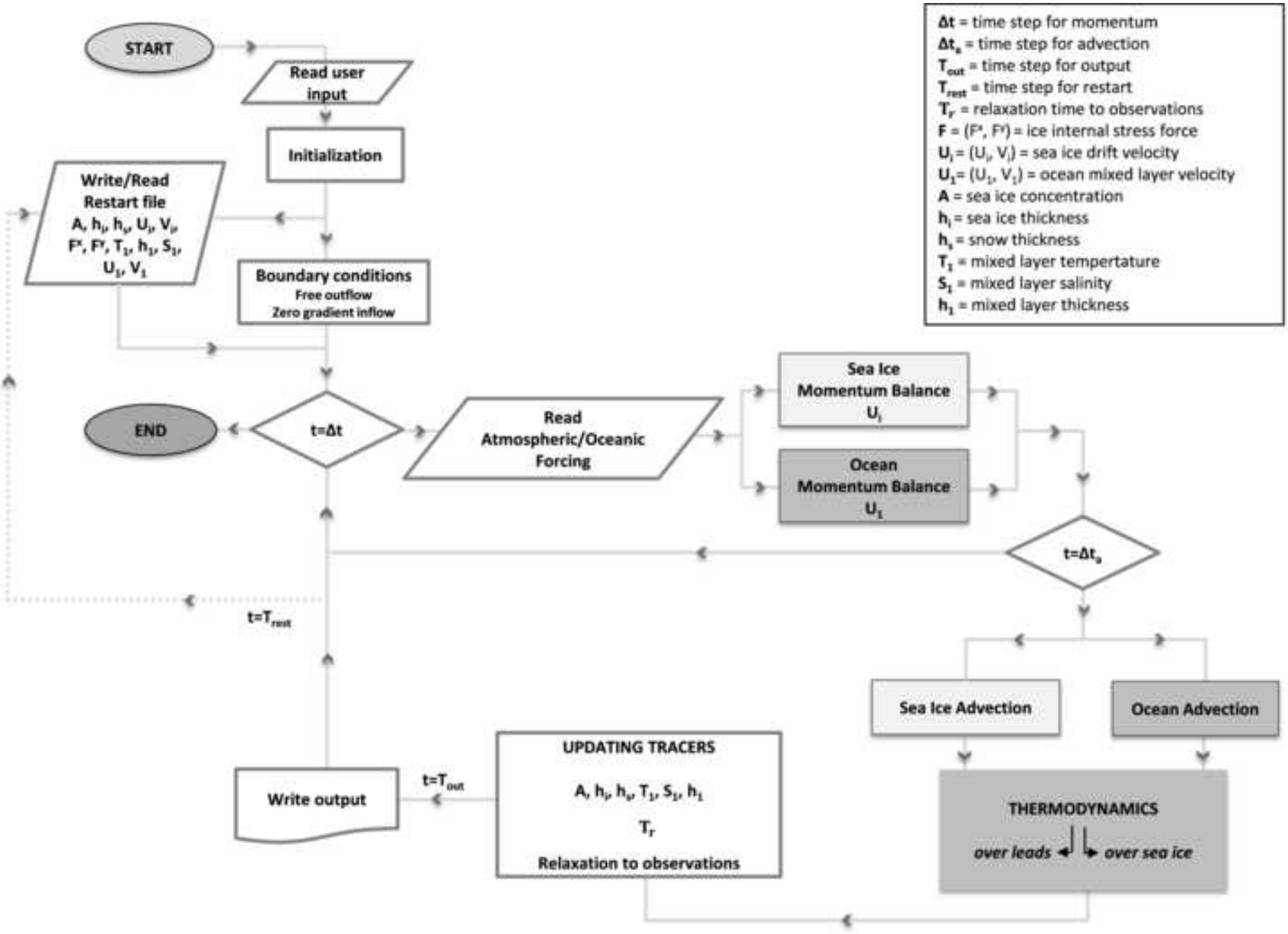

Figure(s)
Click here to download high resolution image

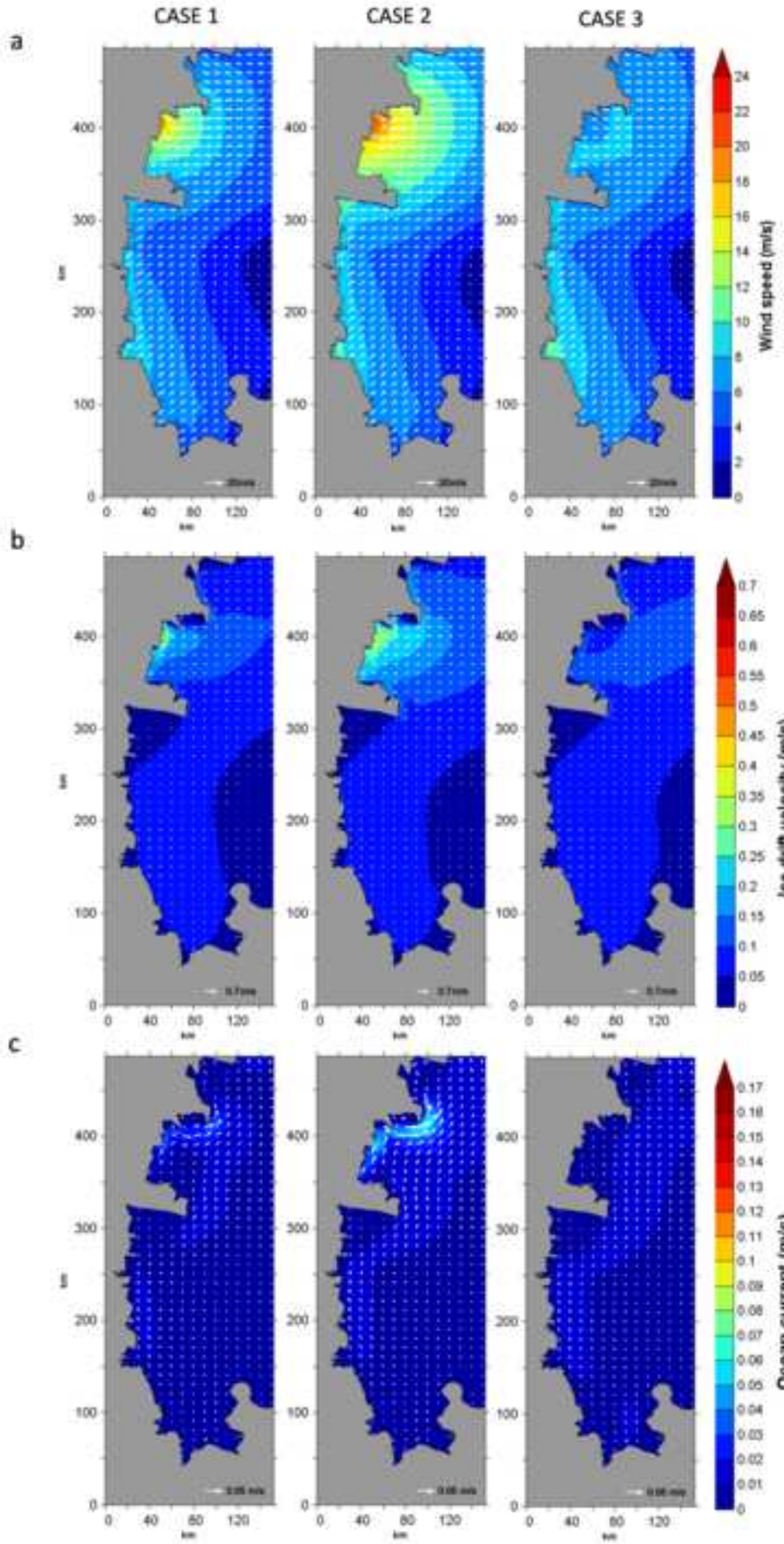

Figure(s)
Click here to download high resolution image

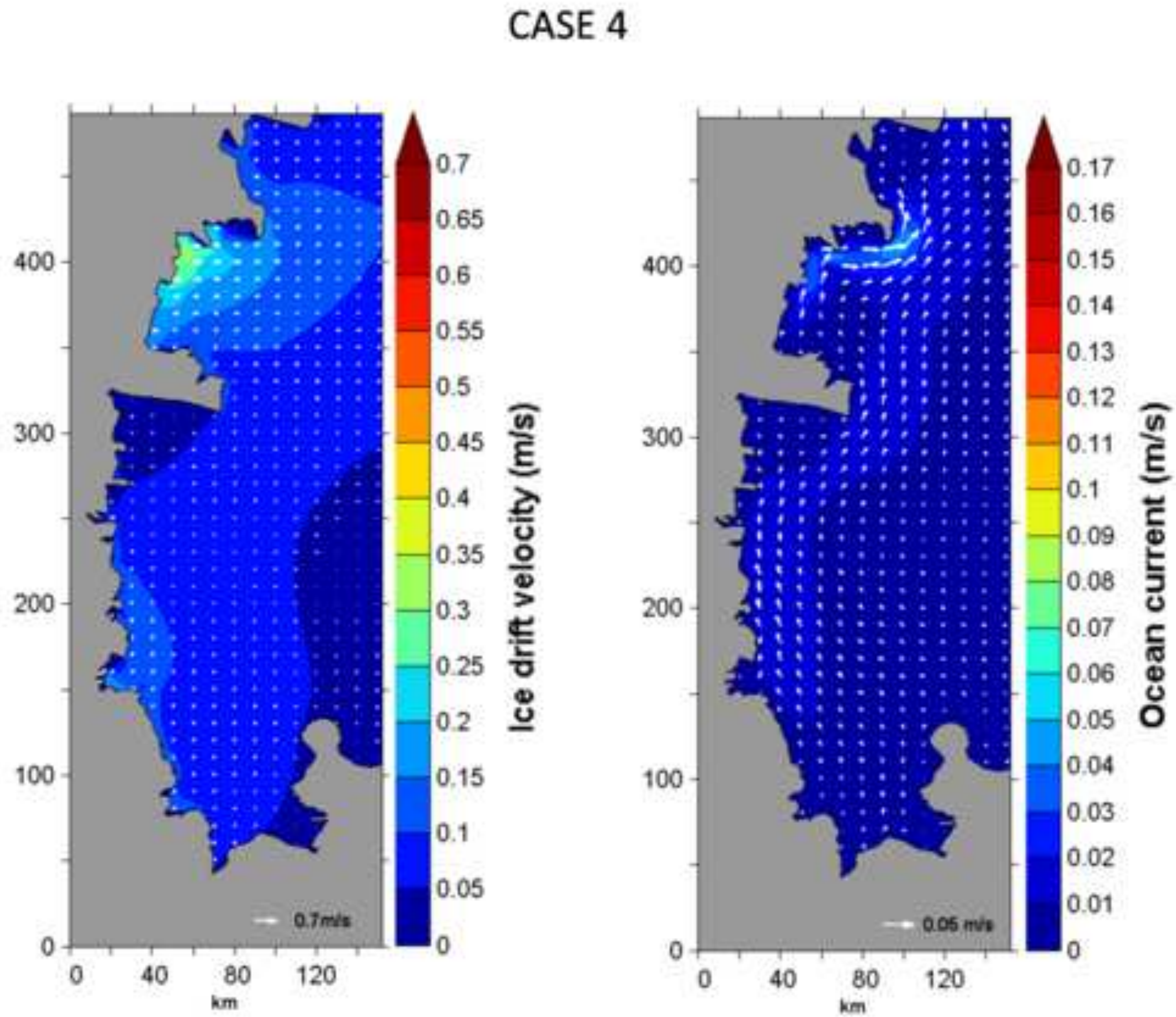

Figure(s)
Click here to download high resolution image

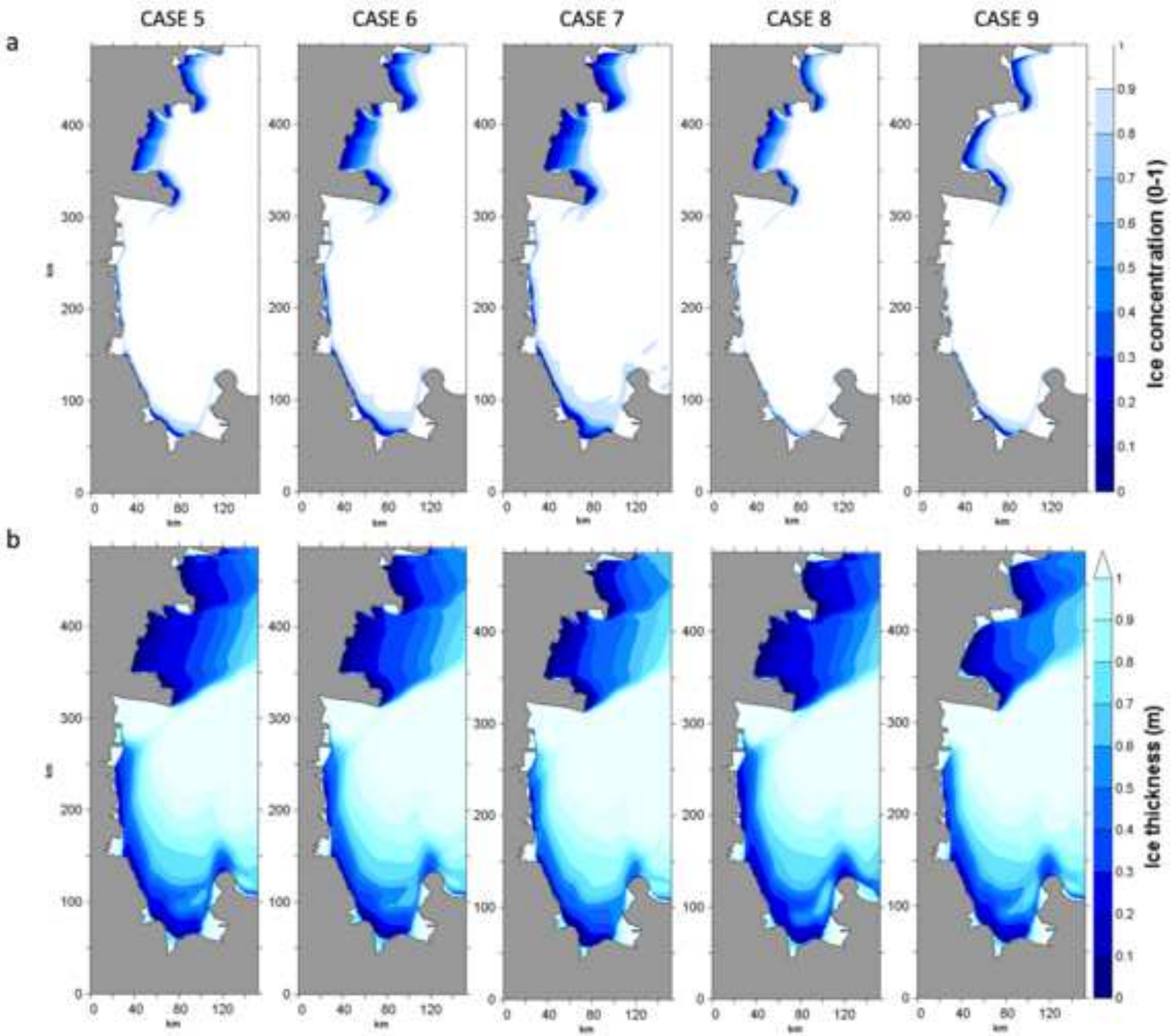

Figure(s)
Click here to download high resolution image

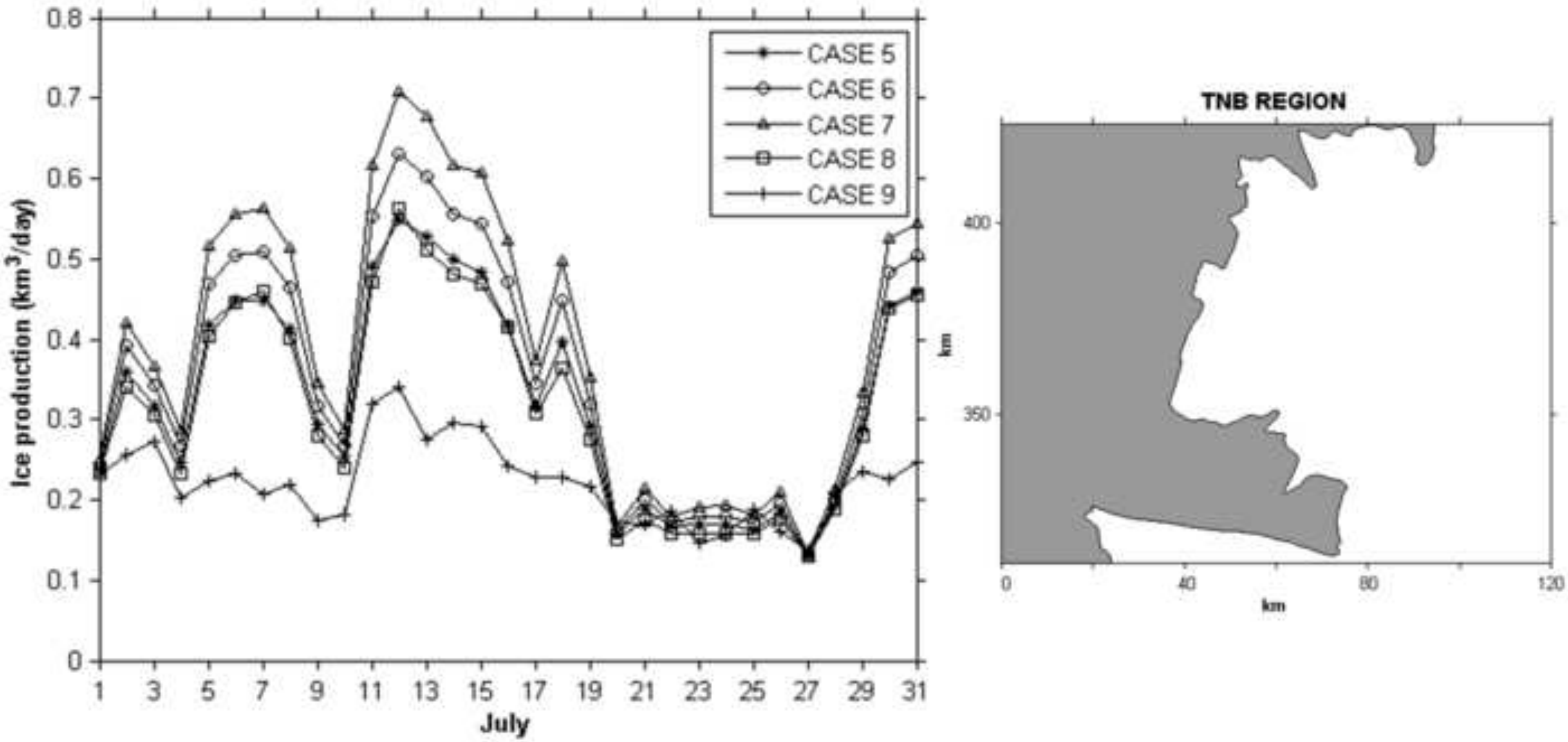

Figure(s)
Click here to download high resolution image

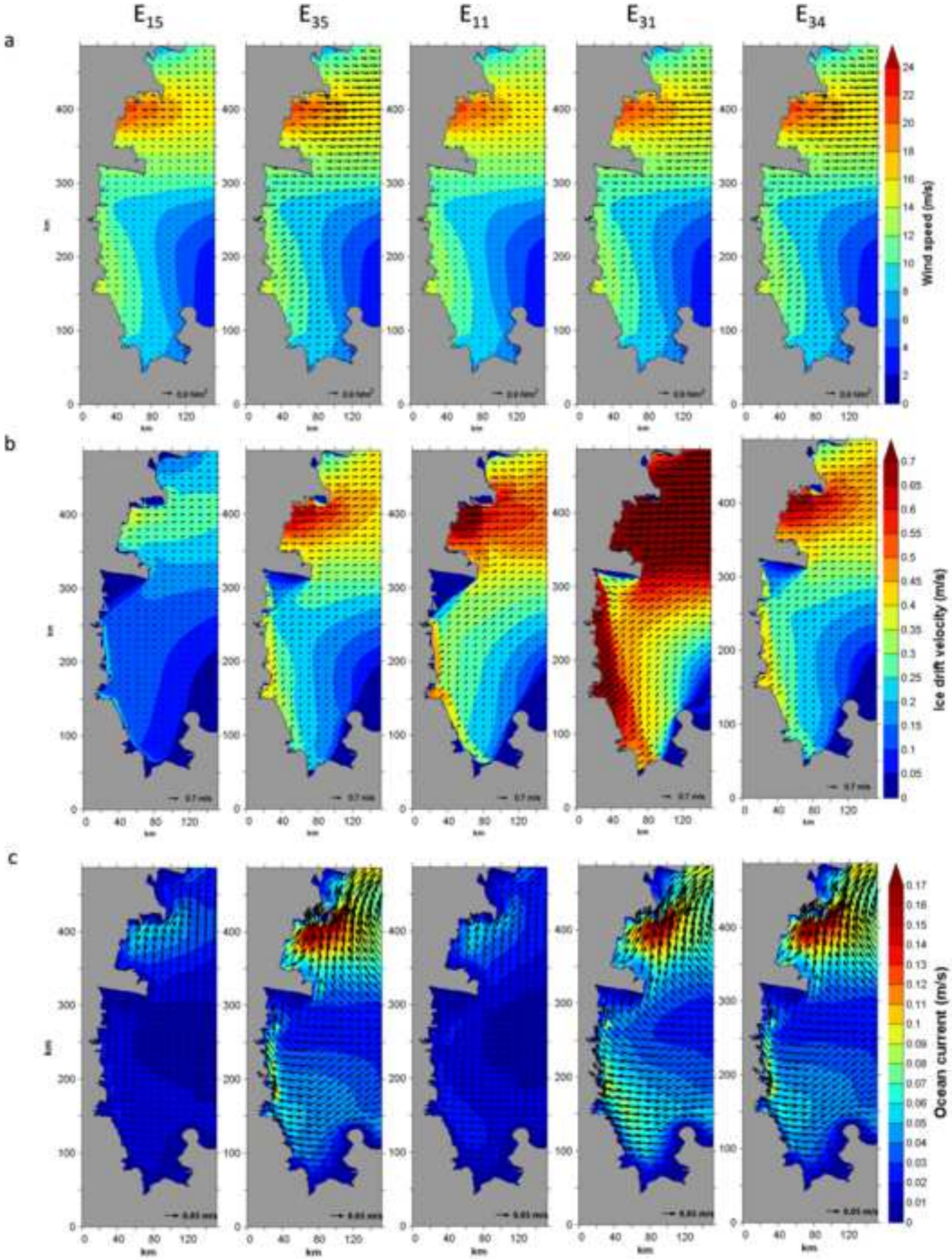

Figure(s)
Click here to download high resolution image

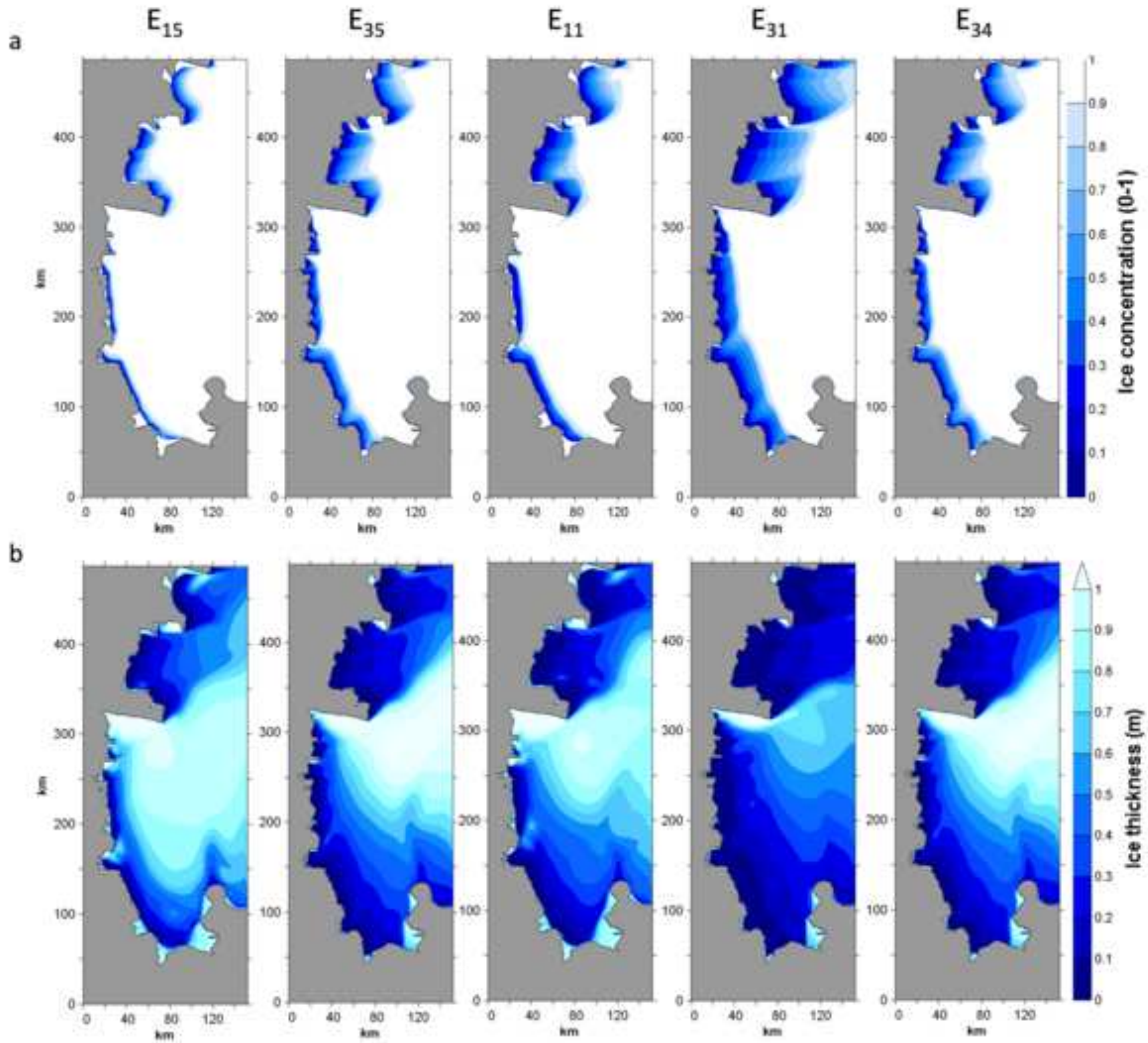

Figure(s)

Click here to download high resolution image

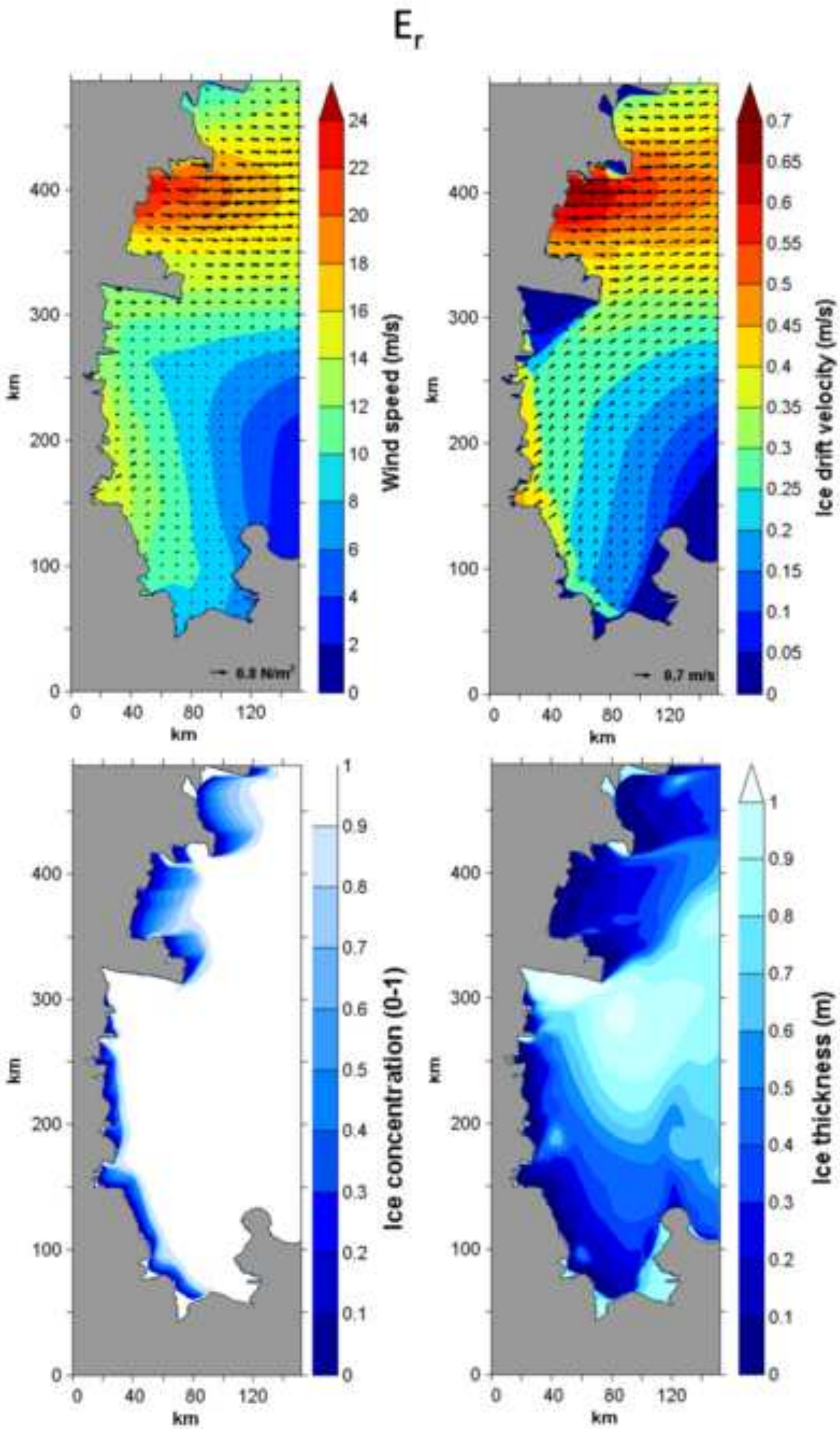

Figure(s)

Click here to download high resolution image

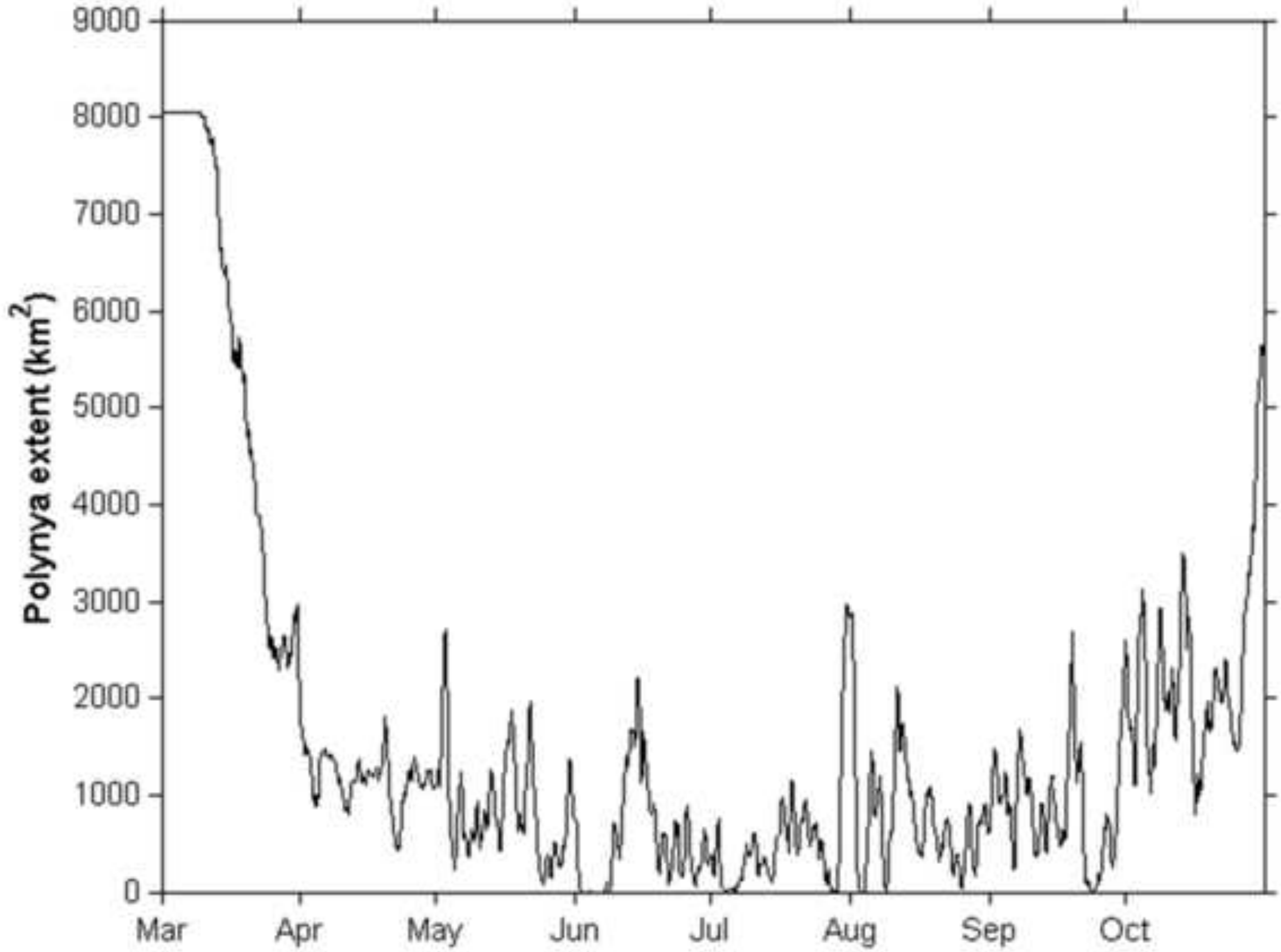

Figure(s)
Click here to download high resolution image

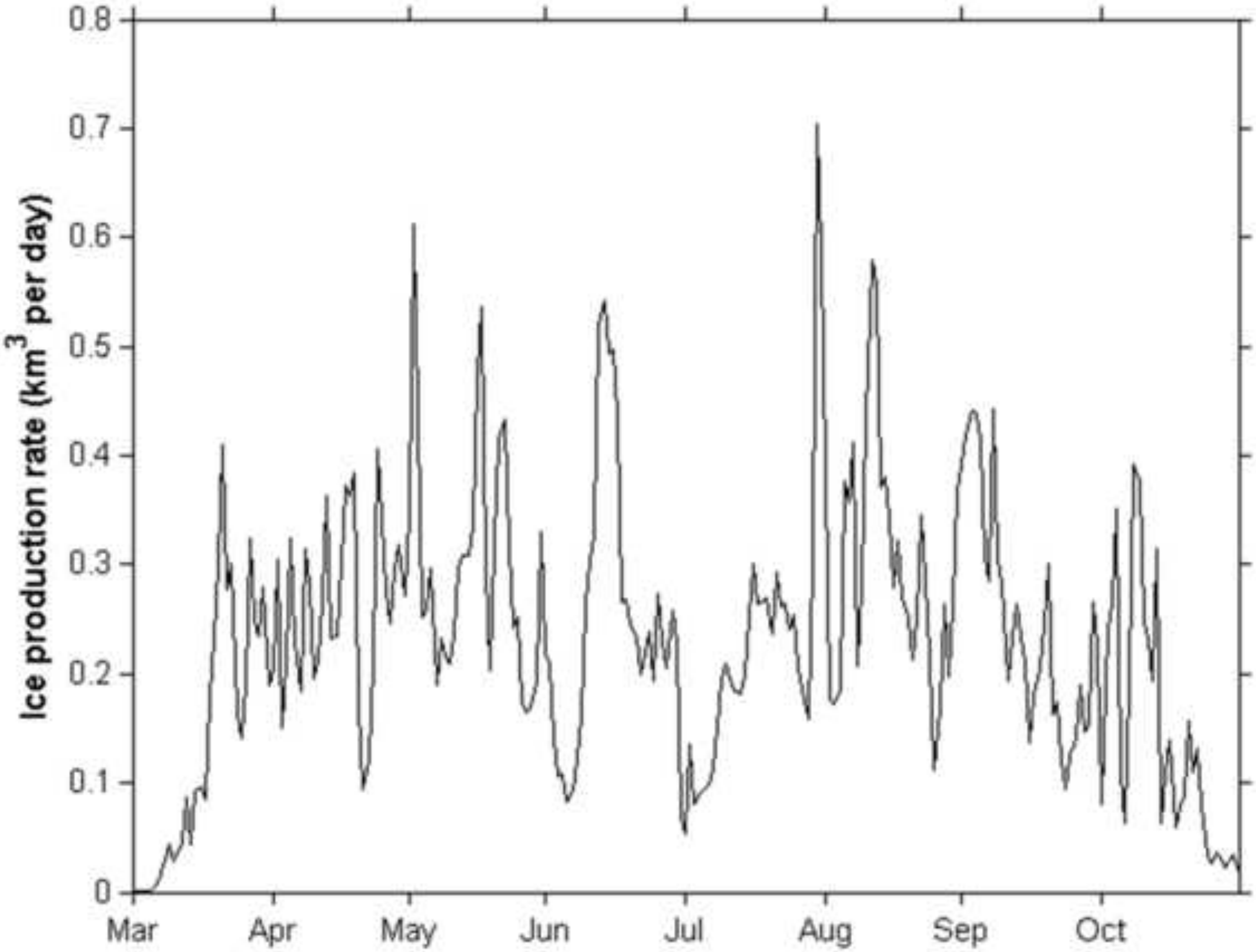

Figure(s)

Click here to download high resolution image

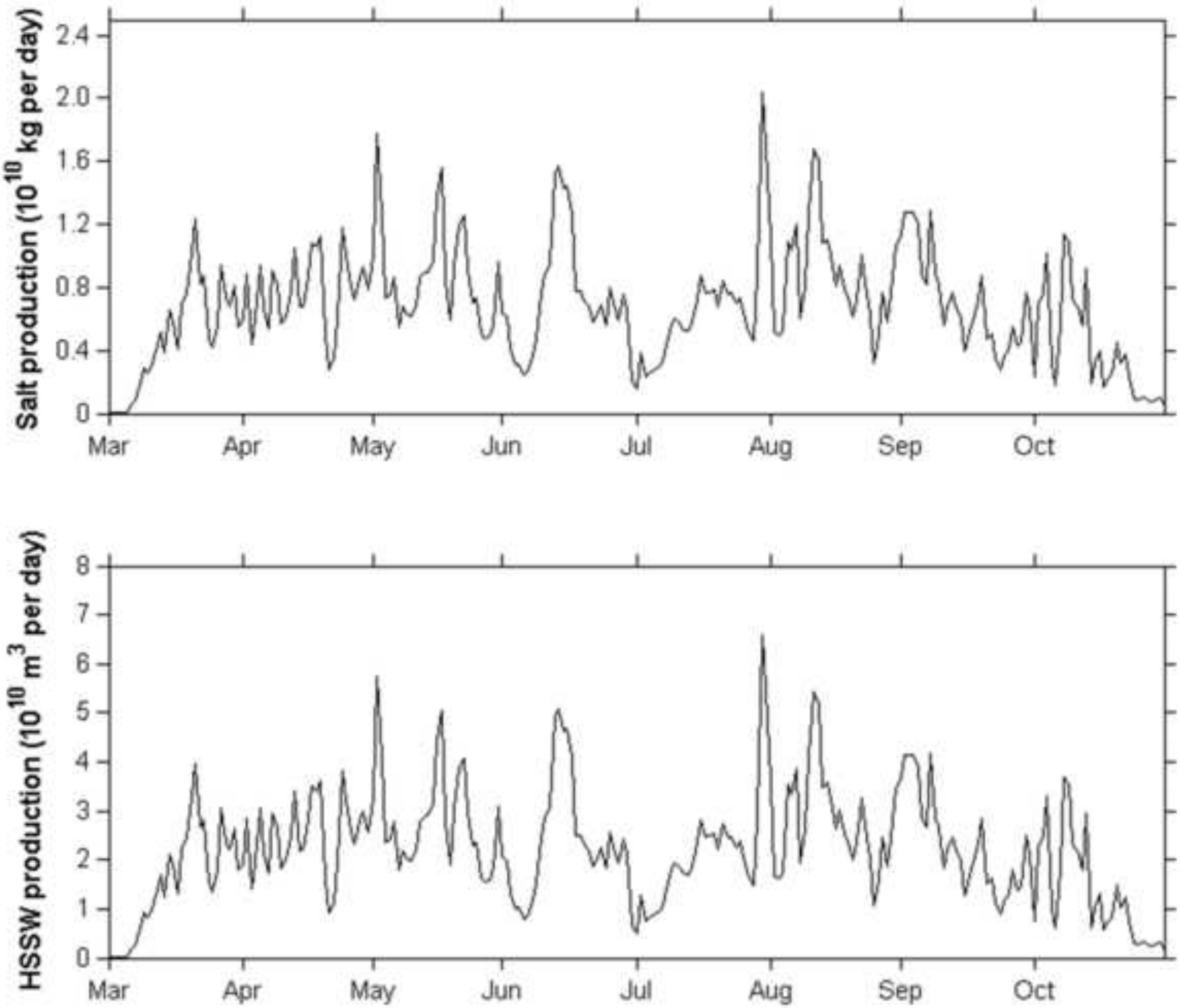

Figure(s)
Click here to download high resolution image

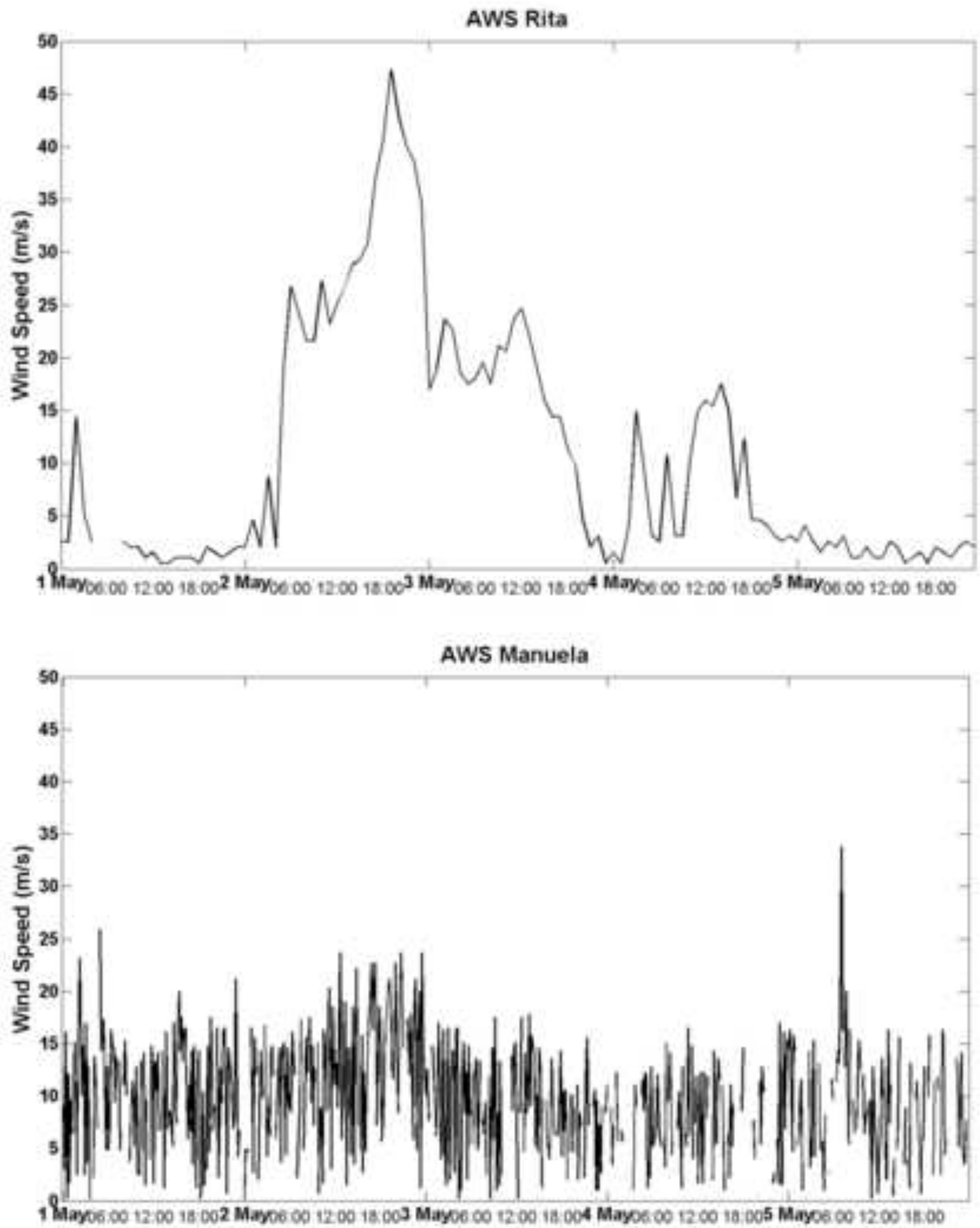

Figure(s)

Click here to download high resolution image

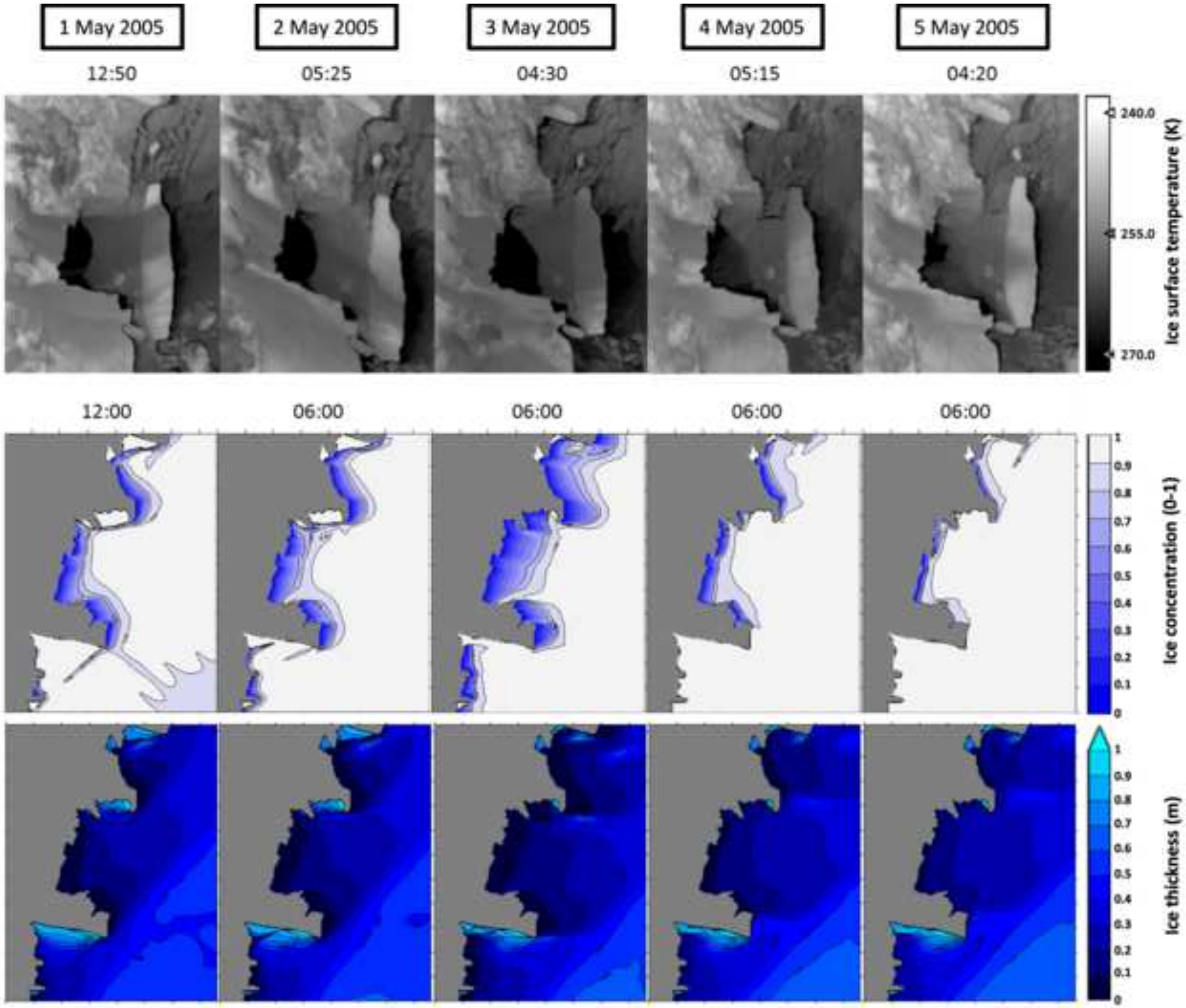

Figure(s)
Click here to download high resolution image

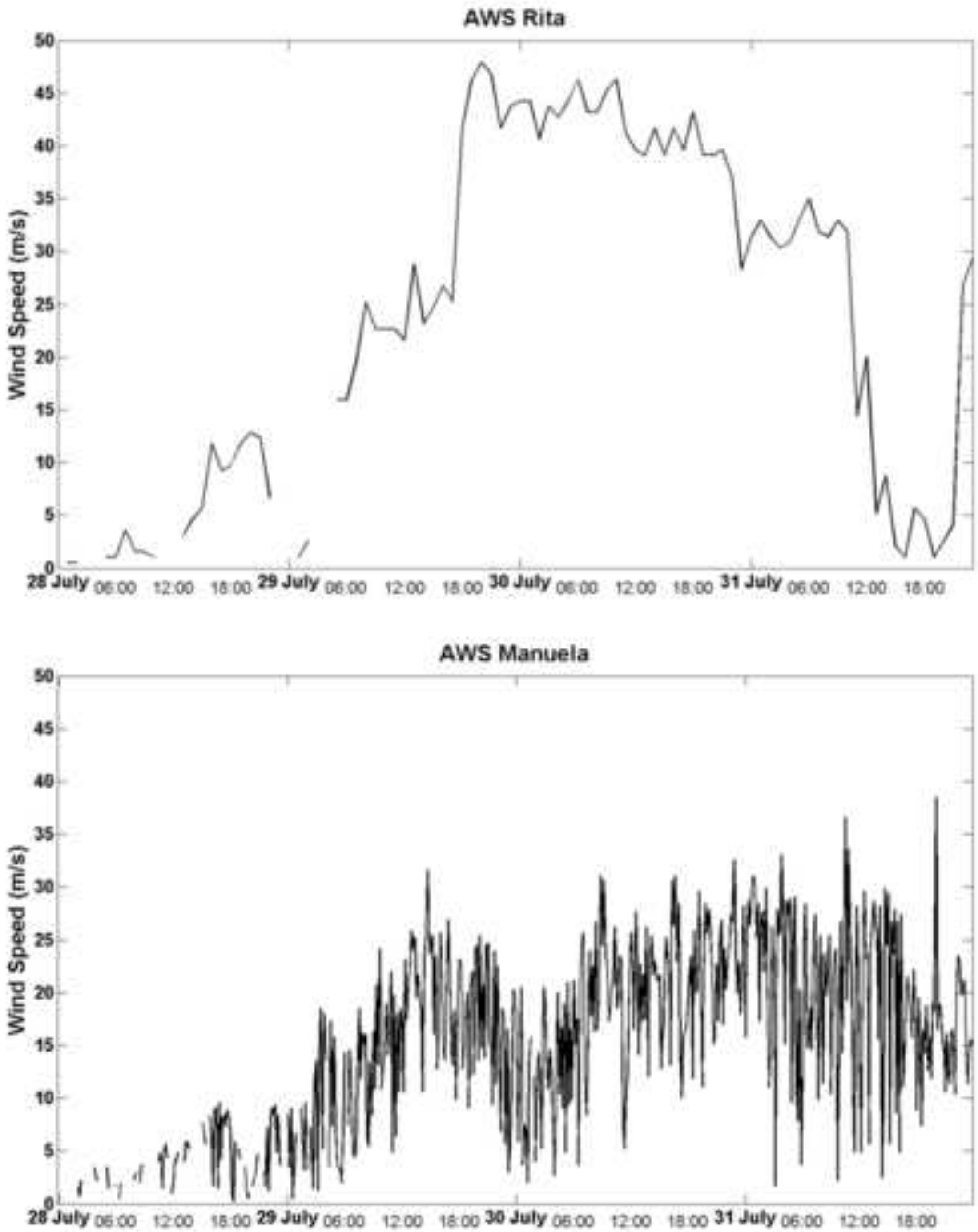

Figure(s)
Click here to download high resolution image

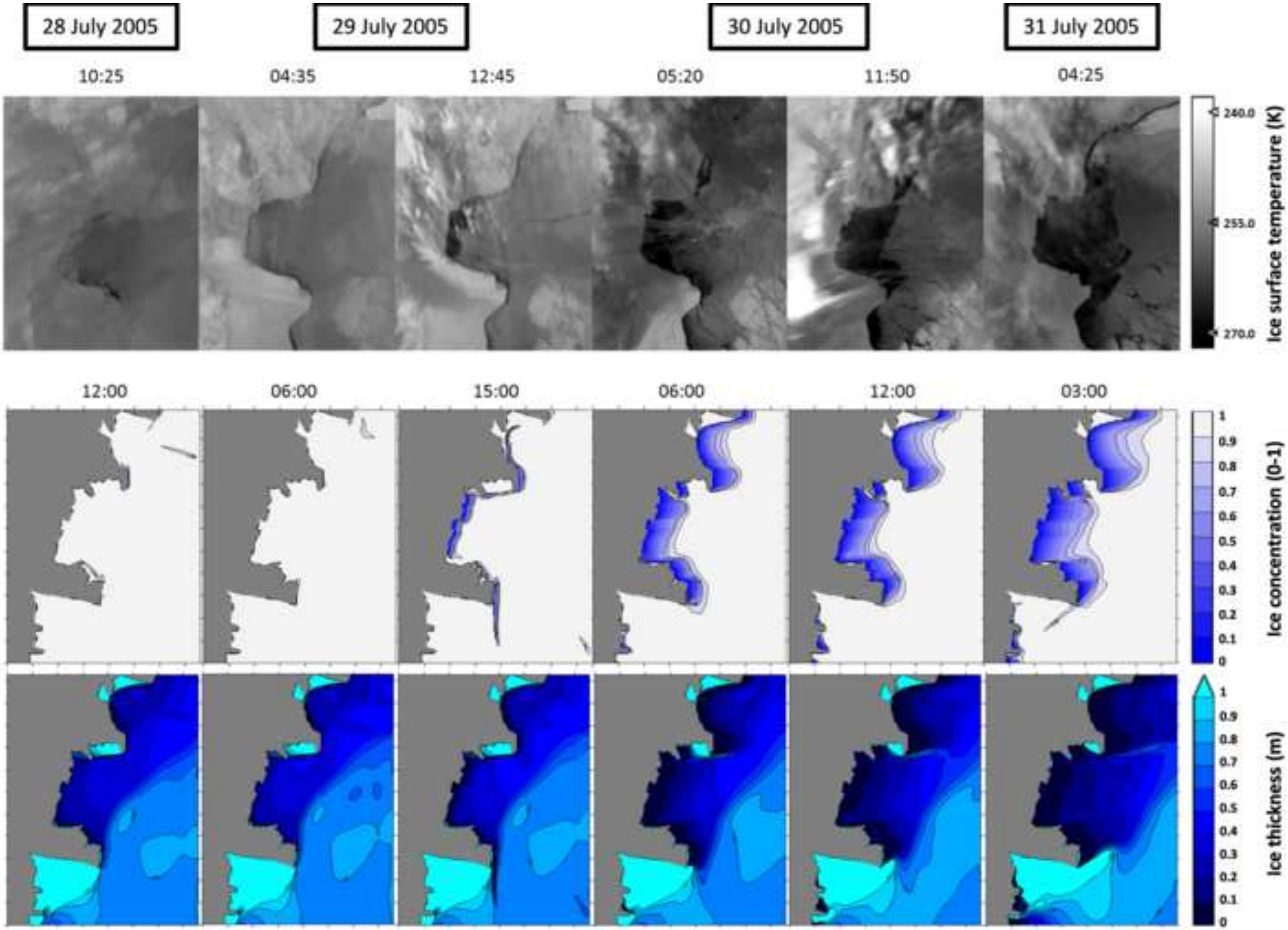

Parameter	**Symbol**	**Value**
X domain	X	154000 m
Y domain	Y	488000 m
T domain	T	x days
Time step for momentum	Δt	1.2 s
Time step for advection	Δt_a	600 s
Elastic timescale (EVP ice rheology)	Δte	180 s
Air drag coefficient	C_{da}	x
Ocean drag coefficient	C_{do}	x
Ice strength parameter	P^*	x N/m^2
Ice concentration parameter	C	20
Creep limit	c	5×10^{-11} 1/s
Eccentricity of the elliptical yield curve	e	2
Demarcation ice collection thickness in leads	H	x m

Table(s)

Click here to download Table(s): Table 2.docx

Parameter	Symbol	Value
Ocean horizontal viscosity	A_H	2×10^2 m^2 s^{-1}
Ocean eddy thickness diffusivity	κ_e	2×10^2 m^2 s^{-1}
Thermal conductivity of sea ice	κ_i	2.2 W/m/K
Thermal conductivity of snow	κ_s	0.3 W/m/K
Emissivity of atmosphere	ε_a	0.95
Emissivity of ocean	ε_o	0.985
Albedo of ocean	α_o	0.07
Albedo of ice	α_i	0.07-0.7
Albedo of snow	α_{sn}	0.85
Latent heat of fusion of ice	L_{fi}	3.34×10^5 J/kg
Latent heat of vaporization of water	L_e	2.5×10^6 J/kg
Latent heat of fusion of snow	L_{fsn}	3.34×10^5 J/kg
Latent heat of sublimation of snow	L_{ssn}	2.834×10^6 J/kg
Specific heat capacity of ocean	c_{pa}	3985 J/kg/K
Specific heat capacity of air	c_{pa}	1004 J/kg/K
Density of air	ρ_a	1.3 Kg/m^3
Density of ice	ρ_i	900 Kg/m^3
Density of snow	ρ_s	330 Kg/m^3
Density of ocean	ρ_o	1024 Kg/m^3
Melting point of freshwater ice	t_{fus}	0°C
Salinity of sea ice	s_i	4
Exchange coeff. for sensible heat (leads/ice)	c_H	1.75×10^{-3}
Exchange coeff. for latent heat over leads	c_E	1.75×10^{-3}
Exchange coeff. for latent heat over ice	c_E	1×10^{-3}
Stefan-Boltzmann constant	K	5.67×10^{-8} W m^{-2} K^{-4}
Minimum vertical viscosity	υ_{min}	1×10^{-3} m^2 s^{-1}
Scale depth of mechanical dissipation	h_w	7 m
Scale depth of convective dissipation	h_c	50 m

Experiment	***R* (km)**
CASE 1	25
CASE 2	50
CASE 3	no merging

Experiment	***H* (m)**	
CASE 5	0.2	
CASE 6	0.3	
CASE 7	0.4	
CASE 8	f (V)	
CASE 9	0.2	no merging

Experiment	Sea ice production (km^3) in July 2000
CASE 5	10.08
CASE 6	11.09
CASE 7	12.12
CASE 8	9.79
CASE 9	6.83

Table(s)

Click here to download Table(s): Table 6.docx

Experiment		C_{da}	C_{do}
E_{15}	CTRL	1×10^{-3}	5×10^{-3}
E_{35}		3×10^{-3}	5×10^{-3}
E_{11}		1×10^{-3}	1×10^{-3}
E_{31}		3×10^{-3}	1×10^{-3}
E_{34}		3×10^{-3}	4×10^{-3}
E_r		1×10^{-3} $V \leq 10$ m/s 3×10^{-3} $V \geq 20$ m/s	$1.3 \times C_{da}$

Winter months	Maximum Polynya extent (km^2)	Mean Polynya extent (km^2)
March	7946	5574
April	1806	1174
May	2688	871.2
June	2205	557.2
July	2962	532.5
August	2868	766.9
September	2674	875.6
October	5637	2304

Winter months	Maximum daily rates of sea ice production (km^3/day)	Mean daily rates of sea ice production (km^3/day)	Monthly cumulative sea ice (km^3)
March	0.42	0.16	4.99
April	0.40	0.26	7.86
May	0.61	0.30	9.25
June	0.54	0.25	7.52
July	0.70	0.22	6.98
August	0.58	0.30	9.39
September	0.44	0.24	7.34
October	0.39	0.14	4.29

TNB polynya event in July 2005	Model-derived polynya extent (km^2)	MODIS-derived polynya extent (km^2)
28th 12:00	12	40
29th 06:00	0	25
29th 15:00	389	391
30th 06:00	1858	1936
30th 12:00	2148	2385
31th 03:00	2831	3393